Fluorescence ratio and photochemical reflectance index as a proxy for photosynthetic quantum efficiency of photosystem II along a phosphorus gradient

Fluorescence ratio and photochemical reflectance index as a proxy for photosynthetic quantum efficiency of photosystem II along a phosphorus gradient

Sebastian Wieneke[1,2*], Manuela Balzarolo[1,3,4], Han Asard[5], Hamada AbdElgawad[5,6], Josep Peñuelas[3,4], Uwe Rascher[7], Arne Ven[2], Melanie S. Verlinden[2], Ivan A. Janssens[2] & Sara Vicca[2]

[1] Remote Sensing Centre for Earth System Research (RSC4Earth, Faculty of Physics and Earth Sciences, University of Leipzig, Leipzig, Germany

[2] Plant and Vegetation Ecology (PLECO), Department of Biology, University of Antwerp, Wilrijk, Belgium

[3] Consejo Superior de Investigaciones Científicas (CSIC), Global Ecology Unit, CREAF-CSIC-UAB, Bellaterra, 08193 Barcelona, Catalonia, Spain

[4] Centre de Recerca Ecològica i Aplicacions Forestals (CREAF), Cerdanyola del Vallès, 08193 Barcelona, Catalonia, Spain

[5] Integrated Molecular Plant Physiology Research (IMPRES), Department of Biology, University of Antwerp, Antwerp, Belgium.

[6] Botany and Microbiology Department, Faculty of Science, Beni-Suef University, Beni-Suef 62511, Egypt

[7] Institute of Bio- and Geosciences (IBG-2): Plant Sciences, Forschungszentrum Jülich GmbH, Leo-Brandt-Str., Jülich, Germany

Corresponding Author: * Sebastian Wieneke, Talstraße 35, 04103 Leipzig, Germany

Email: sebastian.wieneke@uantwerpen.be

Phone: +3232658877

Highlights :

- Fluorescence and photosynthesis were not linearly related across a phosphorus gradient.
- Quantum use efficiency (Φ_{PSII}) could not be predicted from fluorescence yield alone.
- Pigment corrected PRI and fluorescence ratio allowed to estimate Φ_{PSII} at leaf level.

Abstract

Sun-induced chlorophyll fluorescence (SIF) is one of the most promising remote-sensing signals to assess spatio-temporal variation in photosynthesis. Yet, it has been shown that the positive linear relationship of SIF and photosynthesis, often reported from satellite and proximal remote sensing, is mainly driven by the amount of absorbed photosynthetic active radiation (APAR). By normalizing SIF by APAR these structural first-order effects can accounted for and SIF is then reflecting physiological regulation of photosynthetic efficiency. However, because of the confounding contribution of non-photochemical energy dissipation, the relationship between SIF and photosynthetic efficiency is non-linear, and therefore additional measurements have to be included to constrain the predictions of photosynthetic efficiency and photosynthetic electron transport.

We grew *Zea mays* at different phosphorus (P) levels to assess if P-induced reduction in quantum efficiency of PSII (Φ_{PSII}), can be estimated by the fluorescence efficiency parameters, APAR normalized fluorescence (F_{yield}) and the ratio of the two emitted fluorescence peaks ($F_{\uparrow ratio}$), at leaf level. Results were compared to the photochemical reflectance index (PRI), a well-established index related to the activity of the xanthophyll cycle, a protection mechanism which activates under light-stress conditions. We demonstrate that the relationship between Φ_{PSII} and F_{yield} is non-monotonic across a P limitation gradient, rendering the prediction of Φ_{PSII} by F_{yield} alone unfeasible. We show, however, that the pigment corrected PRI (cPRI) and $F_{\uparrow ratio}$ ($cF_{\uparrow ratio}$) share a strong linear relationship with Φ_{PSII}, thereby enabling the estimation of Φ_{PSII}. We demonstrate that a

compensation for reabsorption effects improved the estimation of Φ_{PSII} by F_{ratio} at foliar level. This may allow improved predictions of photosynthetic light use efficiency parameters without the need of measuring green APAR.

Keywords

phosphorus limitation, quantum efficiency of photosystem II, passive fluorescence, sun-induced fluorescence, photochemical reflectance index, non-photochemical quenching

Introduction

Accurate monitoring of photosynthesis (gross primary productivity; GPP) is critical for reliable estimates of crop productivity, stress, or failure, as well as for calibration and validation of land surface models (Ciais *et al.*, 2014). Due to its close link to the photosynthetic process, sun-induced fluorescence (SIF) is one of the most promising signals to assess spatio-temporal variation in GPP remotely (Frankenberg *et al.*, 2011; Guanter *et al.*, 2014; Yang *et al.*, 2015). The often observed linear relationship between SIF and GPP from satellite and proximal remote sensing platforms (e.g. Guanter *et al.*, 2014; Zhang *et al.*, 2016; Cui *et al.*, 2017) are, however, primarily driven by the amount of absorbed photosynthetic active radiation (APAR) (Miao *et al.*, 2018; Yang *et al.*, 2018; Wieneke *et al.*, 2018; Dechant *et al.*, 2020). It is therefore expected that the relationship of APAR normalized fluorescence and photosynthesis better capture the mechanisms of photosynthesis (Magney *et al.*, 2020; Maguire *et al.*, 2020). Due to canopy effects (e.g. Dechant *et al.*, 2020), but also complex non-linear processes at leaf scale (e.g. van der Tol *et al.*, 2014; Maguire *et al.*, 2020), the interpretation of these relationships is still challenging.

The light energy absorbed by chlorophyll can follow three competitive pathways: drive the photochemical reaction (photochemical quenching), be released as heat (non-photochemical quenching; NPQ), or be emitted as fluorescence from both sides of the leaf in the wavelength range of 650 to 800 nm (F_{tot}), with two distinctive peaks at 685 nm (F_{685}) and 740 nm (F_{740}) (Lichtenthaler & Rinderle, 1988). When exposed to excessive light,

plants protect photosystem II (PSII) by releasing energy through NPQ, which consequently reduces photochemical quenching and the quantum efficiency of photosystem II (Φ_{PSII}) (Müller *et al.*, 2001). NPQ and Φ_{PSII} can be derived from pulse amplitude modulated (PAM) fluorometers, which have been used for decades to study photosynthesis at leaf level (Baker, 2008).

Active fluorescence measurements and modeling exercises have shown that the relationship between fluorescence quantum yield and Φ_{PSII} is non-monotonic and driven by changes in NPQ (Maxwell & Johnson, 2000; Baker, 2008; van der Tol *et al.*, 2014; Maguire *et al.*, 2020). Even though previous experiments found such non-monotonic relationship (van der Tol *et al.*, 2014; Pinto *et al.*, 2016; Marrs *et al.*, 2020) no study evaluated all relevant confounding factors, i.e. pigment content, quantitative data on photosynthetic efficiency, the degree of non-photochemical dissipation and fluorescence yield ($F_{yield} = F_{tot}$ / APAR). Due to the complex relationship of F_{yield}, Φ_{PSII} and NPQ and confounding effects of the canopy structure and pigment pools, leaf-level measurements are of utmost importance to improve our understanding about SIF and to establish a functional relationship between SIF and photosynthesis. This is particularly important because SIF is being increasingly used to estimate and interpret photosynthesis in space and time (Wood *et al.*, 2017; Sun *et al.*, 2018; Magney *et al.*, 2019; Mohammed *et al.*, 2019).

Besides nitrogen, phosphorus (P) is one of the two major limiting nutrients for terrestrial plant productivity which can result in photosynthetic downregulation (Hou *et al.*, 2021).

Previous studies have shown that phosphorus limitation of plants can be tracked by active and passive fluorescence measurements (Conroy *et al.*, 1986; Lima *et al.*, 1999; Yaryura *et al.*, 2009; Frydenvang *et al.*, 2015; Migliavacca *et al.*, 2017; Carstensen *et al.*, 2018). Phosphorus deficiency inhibits adenosine triphosphate (ATP) synthase in the light reactions, leading to excessive proton accumulation in the lumen and activation of the xanthophyll cycle. This, in turn, results in an increase of the energy-quenching (qE) component of NPQ and a subsequent reduction in electron transport rate (ETR) of PSII (Carstensen *et al.*, 2018). While NPQ is controlled by the pH gradient between the lumen and thylakoid, fluorescence is not actively regulated and depends on the relationship between NPQ and qE (Porcar-Castell *et al.*, 2014). The activation of the xanthophyll cycle generates an optical reflectance signal that can be detected around 531 nm. The photochemical reflectance index (PRI) exploits these changes in reflectance at 531 nm, relative to a reference wavelength at 570 nm, to assess the activity of the xanthophyll cycle (Gamon *et al.*, 1992; Peñuelas *et al.*, 1995). The PRI and adaptations thereof are considered as the reflectance indices with the closest link to the degree of NPQ (Garbulsky *et al.*, 2011; Vicca *et al.*, 2016; Zhang *et al.*, 2017; Kohzuma & Hikosaka, 2018; Woodgate *et al.*, 2019).

The ratio of the two fluorescence peaks ($F_{\uparrow ratio} = F_{\uparrow 685} / F_{\uparrow 740}$) might be another approach for the quantification of Φ_{PSII} from optical remote sensing. While $F_{\uparrow 685}$ is mainly associated with fluorescence emission of PSII, $F_{\uparrow 740}$ consists of fluorescence emission from PSII and PSI (Buschmann, 2007). With increasing P limitation ETR of PSII decreases

more strongly than ETR of PSI (Carstensen *et al.*, 2018). Consequently, $F_{\uparrow 685}$ is expected to decrease more than $F_{\uparrow 740}$ leading to an overall decrease of the $F_{\uparrow ratio}$ with increasing P limitation. However, since the $F_{\uparrow ratio}$ is strongly affected by reabsorption features of $F_{\uparrow 685}$ the chlorophyll content has to be taken into account when $F_{\uparrow ratio}$ is calculated (Yaryura *et al.*, 2009; Van Wittenberghe *et al.*, 2013).

We created a wide P limitation gradient in a mesocosm experiment with *Zea mays.* The goals of this study were to assess i) if leaf level F_{tot} is linearly related to leaf photosynthesis within a P-limitation gradient, ii) if we can observe a non-monotonic relationship between F_{yield} and Φ_{PSII} as studies with active fluorescence imply, iii) if $F_{yield,}$ the PRI and the $F_{\uparrow ratio}$ are suitable predictors of Φ_{PSII} at leaf level.

Materials and Methods

Experimental setup

Thirty mesocosms (1 m × 1.2 m, 0.6 m high) were set up in a greenhouse in Sint-Katelijne-Waver, Belgium (51.077°N, 4.535°E). The mesocosms were filled with a homogenized, P-poor mixture consisting of pine-forest sand, white river sand, lime and a minority of compost, which was heated at 80 °C for 4 h to ensure the absence of arbuscular mycorrhiza fungi (AMF) (Verlinden *et al.*, 2018), creating a severe P-limiting environment. Each mesocosm was planted with 12 seedlings of maize (*Zea mays* L., variety 'Tom Thumb') on 21 June 2017 and harvested on 31 August 2017. Whereas all mesocosms received ample nitrogen (95.5 kg N ha^{-1}), potassium (79 kg K ha^{-1}), and all micronutrients

142 (in kg ha^{-1}: 19 Mg, 53 S, 0.4 B, 0.1 Cu, 2.4 Fe, 1.1 Mn, 0.1 Mo, 0.4 Zn), triple superphosphate
143 (TSP) phosphate fertilizer was applied at four levels (2.5, 5, 10 and 20 kg P ha^{-1}) to 20
144 mesocosms (five replicates each). Plants in these 20 mesocosms were inoculated with
145 AMF (species Rhizophagus irregularis, Symplanta®). Details about the root colonization
146 can be found in Ven *et al.* (2020) and the supplementary data (Figure S1). TSP was also
147 added at two levels (2.5 and 20 kg P ha^{-1}) to 10 mesocosms without AMF inoculation.
148 Because AMF are especially important in plant P uptake from soils (Marschner *et al.*, 1986;
149 Ge *et al.*, 2000; Liao *et al.*, 2001), we assumed that P deficiency would be most extreme
150 in the non-AMF treatments. Above- and below ground total dry biomass (TB), as well as
151 the carbon (C), nitrogen (N) and P contents of the plant tissues (roots, stems, leaves and
152 cobs) were measured after harvest (71 days after seeding) (Ven *et al.*, 2020).
153 Volumetric soil-water content was monitored (CS650, Campbell Scientific Inc., Logan,
154 USA) in all mesocosms and maintained at a non-limiting (6-12%) level by manual
155 irrigation. Per mesocosm, two recently matured sunlit leaves were selected in each of two
156 measurement campaigns, 27-29 and 57-61 days after seeding (first and second
157 campaigns, respectively). Measurements were conducted between 10 am and 5 pm. In
158 the first measurement campaign, the mean values of temperature and PAR within this
159 time-window were 23.7 °C and 957 µmol s^{-1} m^{-2} respectively, while in the second
160 campaign the mean values were 21.2 °C and 880 µmol s^{-1} m^{-2}. We first measured the CO_2
161 gas exchange and active fluorescence, after a adjustment phase of around 5-10 minutes
162 passive fluorescence and reflectance (R) was obtained for each selected leaf. Finally, the

163 leaves were frozen in liquid nitrogen and analyzed for Chlorophyll a and b, beta-Carotene,
164 and the xanthophyll cycle pigments Violaxanthin, Antheraxanthin and Zeaxanthin
165 (Balzarolo *et al.*, 2018). From the 120 leaf measurements 16 were discarded due to errors
166 in the spectral measurement sequence (measurements with wrong or no short-pass filter)
167 and bad data quality of the gas measurements due to a gasket air leakage. Additional light
168 response curves were measured with a second gas exchange system on one leaf per
169 mesocosm and for both campaigns.
170
171 **Measurement of foliar gas exchange and active fluorescence**
172 Foliar CO_2 gas exchange, light response curves and active fluorescence were measured
173 using a portable gas exchange system (LI-6400, LI-COR, Lincoln, NE, USA) operating with
174 a leaf chamber fluorometer (LI-6400-40). Air flow rate and CO_2 concentration in the leaf
175 cuvette was maintained at 400 µmol mol^{-1} and the block temperature was set at 20°C.
176 Net leaf photosynthesis (A_{net}) and steady-state fluorescence (F_s) were measured at a fixed
177 photosynthetic photon flux density (I) value of 1000 µmol s^{-1} m^{-2}, while the net CO_2
178 exchange at zero light was considered as leaf dark respiration (R_d). Leaves were allowed
179 to equilibrate (5-10 min.) to the described chamber conditions. Gross photosynthesis (A_g)
180 was calculated as:

$$A_g = A_{net} + R_d \quad \text{(E1)}$$

181 Photosynthetic light response curves were obtained by measuring net assimilation rates
182 at light intensities of 0, 20, 50, 100, 250, 500, 1000, 1500 µmol m^{-2} s^{-1} (c.f. Figure S2). The

183 CO_2 concentration in the cuvette was maintained at 400 µmol mol-1 and the block
184 temperature at 20°C. Leaves were allowed to equilibrate at each step before logging the
185 data. The photochemical yield of PSII (Φ_{PSII}), the fraction of absorbed photons by PSII that
186 are used for photochemistry, was inferred from active fluorescence measurements and
187 computed as in Genty *et al.* (1989):

$$\Phi_{PSII} = \left(\frac{F_m{}' - F_s}{F_m{}'}\right) \quad \text{(E2)}$$

188 the maximal fluorescence of the light adapted leaf ($F_m{}'$) was obtained by triggering it with
189 a saturating light flash.

190

191 **Analysis of foliar pigments**

192 Frozen maize leaves were homogenized using a MagNALyser (Roche Diagnostics,
193 Vilvoorde, Belgium) in acetone. The solution was centrifuged (14 000 g, 4 °C, 20 min), and
194 the supernatant filtered (Acrodisc GHP filter, 0.45 µm 13 mm), and analyzed by high-
195 performance liquid chromatography HPLC (Shimadzu SIL10-ADvp, reversed-phase, at 4
196 °C) (Thayer & Björkman, 1990). Carotenoids (Car) were separated on a silica-based C18
197 column (Waters Spherisorb, 5 µm ODS1, 4.6 × 250 mm, with solvent A 81:9:10
198 acetonitrile:methanol:water and solvent B 68:32 methanol:ethyl acetate. Chlorophyll a
199 and b, beta-carotene and xanthophylls were detected using a diode-array detector
200 (Shimadzu SPD-M10Avp) at four wavelengths (420, 440, 462, 660 nm). Concentrations
201 were determined using the Shimadzu Lab Solutions Lite software, and a calibration curve
202 (Balzarolo *et al.*, 2018).

The epoxidation state (EPS) of the xanthophyll pigments, a group of carotenoid pigments (Violaxanthin, V; Antheraxanthin, A; Zeaxanthin, Z) which are involved in the heat dissipation mechanism of the pH- or energy-dependent form of non-photochemical quenching (qE) was calculated as:

$$EPS = \frac{\left(V + \frac{A}{2}\right)}{(V + A + Z)} \quad \text{(E3)}$$

For plants containing VAZ pigments, excessive light conditions lead to proton accumulation within the chloroplast lumen, resulting in its acidification and the activation of the xanthophyll cycle. By de-epoxidating the diepoxide violaxanthin via the monoepoxide antheraxanthin to the epoxide-free form zeaxanthin, excessive energy can be released as heat. Hence, low values of EPS indicate high qE activity when plants emit more energy as heat and reduce their Φ_{PSII}.

Measurement of passive foliar fluorescence and reflectance

After measuring gas exchange and active fluorescence, passive fluorescence and reflectance were immediately measured using a FluoWat leaf clip (for a detailed description c.f. Van Wittenberghe *et al.*, 2013) connected to a spectroradiometer (spectral resolution: 3 nm, spectral range: 325–1075 nm, ASD FieldSpec, Malvern Panalytical, Boulder, USA). To ensure a fast and continuous measurement cycle and to avoid damage to the maize plants within the mesocosm, the leaves were cut right before the FluoWat measurements. With the cutting of the leaf the stomata will start to close and thereby reduce photosynthesis within several minutes (Le *et al.*, 2011; Daszkowska-

223 Golec & Szarejko, 2013). Since the leaf was measured 60 to 90 seconds after cutting, we
224 do not expect an effect on the reflectance (Foley *et al.*, 2006) and only a minor influence
225 on the passive fluorescence measurements (Rajewicz *et al.*, 2019). The FluoWat leaf clip
226 was carefully positioned over the same area of the leaf where gas exchange was
227 measured. The design of the FluoWat allows observing the leaf at the nadir from upward
228 and downward positions, where the light falls on the leaf at 45°. Reflectance (R) and
229 transmittance (T) were measured using upward and downward fiber-optic insertions. A
230 short-pass filter that blocks light at wavelengths >650 nm was moved in front of the
231 incident light to obtain upward and downward emitted F ($F_{\uparrow}$ and $F_{\downarrow}$, respectively). Due
232 to cloudy weather conditions during both campaigns, the FluoWat was used in
233 combination with an artificial light source (ASBN-W, Spectral Products, Connecticut,
234 Putnam, USA; PPFD of 596±28.9 µmol m^{-2} s^{-1}). To allow a comparison of Φ_{PSII}
235 measurements (performed at 1000 µmol m^{-2} s^{-1}) with passive fluorescence (performed at
236 600 µmol m^{-2} s^{-1}), a transfer function derived from campaign- and treatment- specific light
237 response curves (c.f. Figure S2), was used to recalculate Φ_{PSII} to 600 µmol m^{-2} s^{-1}. These
238 values where then used for the subsequent analyses.
239 Reflectance, transmittance and F are thus obtained for the same area of the leaf in one
240 measurement cycle (Van Wittenberghe *et al.*, 2013). The photochemical reflectance index
241 (PRI) for the acquired foliar-reflectance spectra was calculated as:

$$PRI = \frac{R_{570} - R_{531}}{R_{570} + R_{531}} \quad \text{(E4)}$$

where the reflectance of green leaves at 531 nm (R_{531}) can be related to the EPS of the xanthophyll cycle and the reflectance at 570 nm (R_{570}) is utilized as a reference wavelength (Gamon *et al.*, 1992). We used the original PRI equation (E4) where an increased PRI indicates an increased release of excess energy by the energy- or pH-dependent (qE) component of non-photochemical quenching (NPQ). Where non-photochemical quenching is composed of qE, photoinhibition (qI) and state-transition (qT) (Müller *et al.*, 2001):

$$NPQ = qE + qI + qT \quad \text{(E5)}$$

To avoid negative PRI values, scaled PRI (sPRI) (Rahman *et al.*, 2004) was calculated as:

$$sPRI = \frac{(PRI + 1)}{2} \quad \text{(E6)}$$

Several studies reported that seasonal changes in foliar pigments affect the relationship between PRI and non-photochemical quenching (Peñuelas *et al.*, 1997; Gamon *et al.*, 2001; Sims & Gamon, 2002; Filella *et al.*, 2009; Rahimzadeh-Bajgiran *et al.*, 2012; Gitelson *et al.*, 2017b). Wong & Gamon (2015) showed that that the PRI changes linearly with the ratio of carotene (Car) to total chlorophyll (Chl). Since this may lead to misinterpretation of PRI as an indicator of qE (Gitelson *et al.*, 2017a; Alonso *et al.*, 2017), we corrected sPRI (cPRI) by normalizing for the carotene to total chlorophyll ratio (Car:Chl).

$$cPRI = \frac{sPRI}{Car{:}\,Chl} \quad \text{(E7)}$$

Two different cPRI were calculated: one based on the measured Car:Chl (cPRI, E7), and another where Car:Chl was derived from its linear relationship with a vegetation index ($cPRI_{vi}$). We tested the performance of several vegetation indices in predicting Car:Chl (c.f.

Table S4) and found that an adapted version of the carotenoid/chlorophyll ratio index (CCRI; (Zhou *et al.*, 2019; Gitelson, 2020) performed best (R^2 = 0.60, c.f. Figure S5c). In its original version the CCRI is calculated as a ratio of the carotenoid index CARI = (R_{720}-R_{521})/R_{521} (Zhou *et al.*, 2017) and the red-edge chlorophyll index $CI_{red\text{-}edge}$ = ($R_{780\text{-}800}/R_{700}$)-1 (Gitelson *et al.*, 2003). While in this study the $CI_{red\text{-}edge}$ showed a strong correlation with Chl (R^2 = 0.98, c.f. Figure S5a), we found that the red-edge carotenoid index $CAR_{red\text{-}edge}$ = $((R_{510})^{-1} – (R_{700})^{-1})\cdot R_{770}$ (Gitelson *et al.*, 2006) performed best in estimating the observed relatively low carotenoid contents (R^2 = 0.89, c.f. Figure S5b, Table S4). Accordingly, we adapted the CCRI (aCCRI) as follows:

$$aCCRI = \frac{CAR_{red-edge}}{CI_{red-edge}} \quad \text{(E8)}$$

The total amount of fluorescence emitted by the leaf (F_{tot}, W m^{-2} sr^{-1}) was calculated from the spectral integral of $F_{\uparrow}$ and $F_{\downarrow}$ between 650 and 800 nm as:

$$F_{tot} = F_{\uparrow} + F_{\downarrow} \quad \text{(E9)}$$

F efficiency (F_{yield}, %), was derived by normalizing F_{tot} by APAR (the product of photosynthetically active radiation between 400 and 700 nm (PAR, W m^{-2}) and the fraction of PAR absorbed by the leaf ($fPAR$) to improve comparison of the measurements:

$$F_{norm} = \frac{F_{tot} \cdot \pi}{fPAR \cdot PAR} \cdot 100 \quad \text{(E10)}$$

where PAR was derived from white reference measurements. Since the Teflon based white reference is not 100% reflective and a fraction of the light is transmitted (around

277 5%), we corrected PAR by accounting for the white reference transmittance measured for
278 each white reference measurement cycle. fPAR was calculated as:

$$fPAR = 1 - R - T \quad \text{(E11)}$$

279 To analyze how an increase in P limitation, and resulting changes in leaf absorption and
280 scattering properties, affect the bi-directional emission of red and far-red fluorescence
281 (Van Wittenberghe *et al.*, 2015) we calculated the contribution of $F_{\uparrow}$ to total F ($F_{\uparrow\%}$, %)
282 as:

$$F_{\uparrow\%} = \frac{F_{\uparrow}}{(F_{\uparrow} + F_{\downarrow})} \cdot 100 \quad \text{(E12)}$$

283

284 **Semi mechanistic model for estimating Φ_{PSII} by $cF_{\uparrow ratio}$**

285 The peak ratio of fluorescence emitted by the adaxial surface of the leaf ($F_{\uparrow ratio}$) was
286 calculated as:

$$F_{\uparrow \mathrm{ratio}} = \frac{F_{\uparrow 685}}{F_{\uparrow 740}} \quad \text{(E13)}$$

287 Where the first peak of fluorescence is located at 685 nm ($F_{\uparrow 685}$) and the second peak at
288 740 nm ($F_{\uparrow 740}$). To compensate for chlorophyll related reabsorption effects of $F_{\uparrow 685}$ a
289 corrected $F_{\uparrow ratio}$ ($cF_{\uparrow ratio}$) was calculated as:

$$cF_{\uparrow \mathrm{ratio}} = \frac{F_{\uparrow 685} \cdot cf}{F_{\uparrow 740}} \quad \text{(E14)}$$

290 Where the correction factor (cf) was calculated from the exponential relationship (R^2 =
291 0.88) between leaf transmittance in the red (TR_{685}) and the vegetation index $CI_{red\text{-}edge}$:

$$cf = \frac{1}{0.02 + 0.0003 \cdot CI_{red-edge}{}^{-2.2}} \quad \text{(E15)}$$

292

293 **Statistical analysis**

294 Data normality and homoscedasticity were verified using Shapiro-Wilk and Levene tests,
295 respectively. A two-way analysis of variance (ANOVA) was applied to determine if the
296 variables differed between treatments and campaigns, where non-normally distributed
297 parameters were log-transformed. A two-sided t-test was applied for pairwise
298 comparison when the effects of a factor were significant (c.f. Table S2 & Table S3). To
299 evaluate if the relationship between Φ_{PSII} and the $cF_{\uparrow ratio}$ is affected by their covariation
300 with Chl and if the relationship between EPS, sPRI, cPRI and $cPRI_{vi}$ is affected by the
301 Car:Chl, a partial correlation was used to determine the strength of their linear
302 relationships while controlling for the Chl and the Car:Chl content as the covariate,
303 respectively.
304 The statistical analysis was performed in Python, using the packages pandas (McKinney,
305 2010), numpy (Harris *et al.*, 2020), scipy (Virtanen *et al.*, 2020) and sklearn (Pedregosa *et*
306 *al.*, 2011).

307

308 **Results**

309 **Biomass distribution and foliar N:P ratio at the end of the season**

310 Total biomass (TB) at the end of the experiment indicated that P limitation strongly
311 affected plant growth: as P supply declined, TB decreased exponentially (Figure 1a). The

treatments with lowest P and no AMF (P1S) showed the lowest biomass and several plants in these mesocosms died prematurely (i.e., before producing seeds). The more than 50% reduction in the P4S treatment (relative to P4) highlights the importance of AMF for these plants, even under well-fertilized conditions. Foliar N:P ratios stabilized near 7 for all mesocosms with active AMF, but were much higher for the mesocosms without AMF (≈ 14 and 21 for P4S and P1S, respectively) (Figure 1b), indicating increased P shortage. Because several plants in P1S senesced and died prematurely, we omitted the P1S treatment from the biomass distribution analysis (Figure 1c).

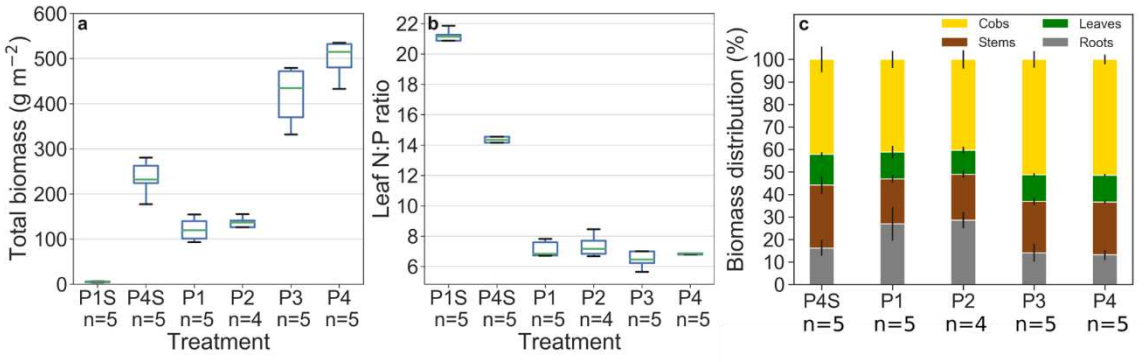

Figure 1: Total biomass (a), foliar N:P ratio (b) and biomass distribution (c) of the maize plants at harvest. P1, P2, P3 and P4 indicate treatment with 2.5, 5, 10 and 20 kg P ha^{-1} triple superphosphate, respectively. P1S and P4S were pasteurized to ensure the absence of arbuscular mycorrhizal fungi. Sample size is indicated by n.

Composition of foliar pigments under P limitation

All foliar pigment contents exhibited the same patterns in both campaigns. Chl a&b, beta-carotene and VAZ contents during the first campaign were higher for the highest P-fertilization treatments (P3, P4 & P4S) and the lowest for the lowest P-fertilization treatments (P1, P2 & P1S) (Figure 2a & Figure S3a, b, c, d). Foliar pigment concentrations

during the second campaign were lower in the pasteurized mesocosms (P4S & P1S) than in their AMF inoculated counterparts with low- (P1 & P2) and, in particular, high P-fertilization (P3 & P4) (Figure 2e & Figure S3e, f, g, h). In both campaigns the Car:Chl ratio increased with P-fertilization (Figure 2b&f), but with overall higher values during the second campaign. The Chl content of P1 and P2 showed no significant difference with each other in both campaigns. However the Car:Chl and VAZ:Chl ratio increased more for P2 than for P1, indicating a stronger investment into carotenoids (Figure 2a, b, e, f). The ratio between the contents of xanthophyll and Chl pigments in both campaigns was the lowest in the pasteurized mesocosms and increased with increasing P-fertilization (Figure 2c & g). During the first campaign also the epoxidation state (EPS) increased with the increasing rate of P-fertilization and AMF presence (Figure 2d). EPS during the second campaign was very high (except for P1S), with low variability among treatments (Figure 2h).

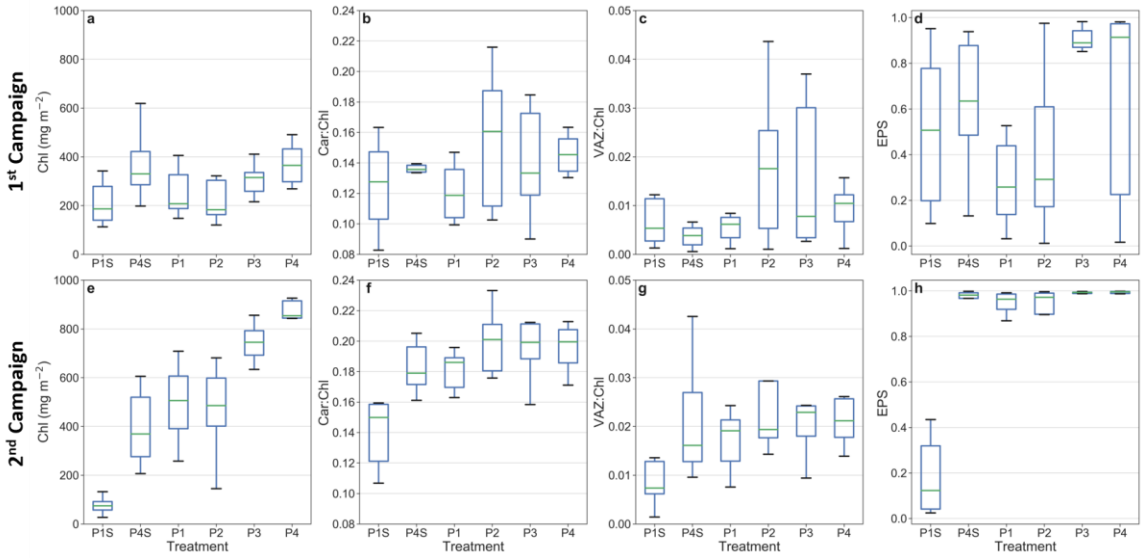

Figure 2: Box plots of total chlorophyll content (Chl), the ratio between carotenoids and total chlorophyll (Car:Chl), the ratio of the total xanthophyll pigment content to total chlorophyll (VAZ:Chl) and the epoxidation state (EPS) 27-29 days after seeding (DAS, first campaign) a-d, and 57-61 DAS (second campaign) e-h. P1, P2, P3 and P4 indicate treatment with 2.5, 5, 10 and 20 kg P ha^{-1} triple superphosphate, respectively. P1S and P4S were pasteurized to ensure the absence of arbuscular mycorrhizal fungi.

Photosynthesis and $F_{\uparrow\%}$ under P limitation

Our experiment produced a wide range of leaf photosynthesis (A_g) and photochemical yield of PSII (Φ_{PSII}) values, with a strong inter-treatment variability. During the first campaign, A_g and Φ_{PSII} were higher in the high P-fertilization treatments (P3, P4 & P4S) than in the low P-fertilization treatments (P1, P2 & P1S) (Figure 3a, b). A different pattern appeared during the second campaign, in which A_g and Φ_{PSII} were similar across all treatments with AMF (P1 to P4), but much lower in the absence of AMF (P4S & P1S versus P1 to P4) (Figure 3e, f).

During the first campaign fPAR was relatively similar across treatments and only during the second campaign a treatment effect emerged; fPAR then decreased with increasing P

limitation and decreasing total chlorophyll content (Figure 3d, h). $F_{\uparrow\%}$ declined from around 65% to 50% with increasing P limitation. During the second campaign, treatment differences had disappeared in the presence of AMF, while the treatments without AMF still exhibited low $F_{\uparrow\%}$ (Figure S4).

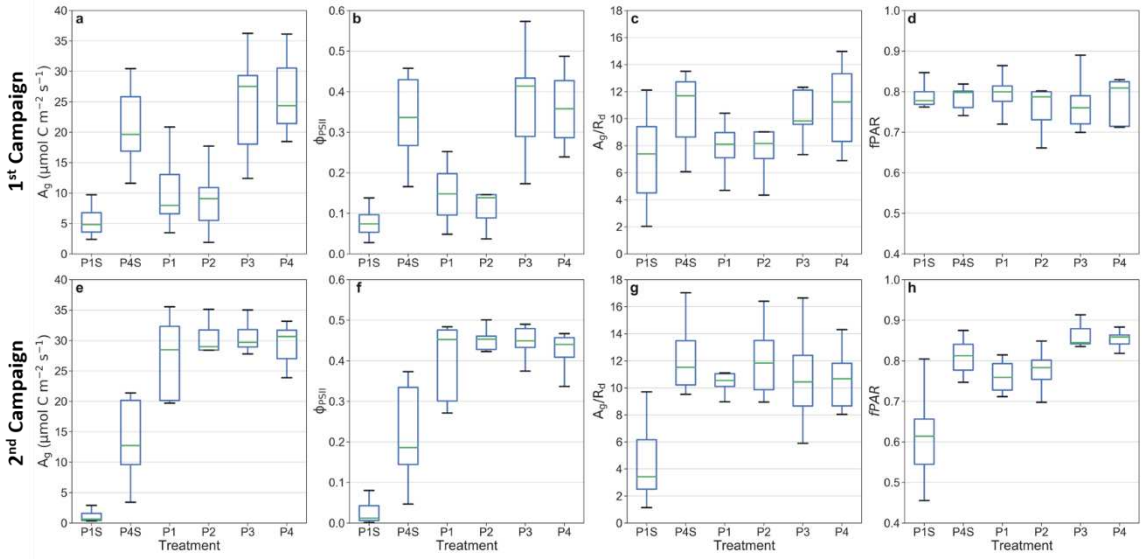

Figure 3: Box plots of gross photosynthesis (Ag), quantum efficiency of PSII (ΦPSII)), ratio of Ag to dark respiration (Rd) and the fraction of absorbed photochemical active radiation (fPAR). 27-29 days after seeding (DAS, first campaign) a-d and 57-61 DAS (second campaign) e-h. P1, P2, P3 and P4 indicate treatment with 2.5, 5, 10 and 20 kg P ha^{-1} triple superphosphate, respectively. P1S and P4S were pasteurized to ensure the absence of arbuscular mycorrhizal fungi.

Estimation of EPS by cPRI

Across treatments and campaigns, EPS showed a strong positive relationship with Φ_{PSII} (Figure 4a). The scaled PRI (sPRI) showed a strongly decreasing linear relationship with EPS (Figure 4b), where the Car:Chl normalized sPRI (cPRI) greatly improved the prediction of EPS, with R^2 = 0.82 and a *rRMSE* = 13.3%. Compared to the performance of sPRI the reflectance based $cPRI_{vi}$ was also a better predictor of EPS, albeit less than cPRI (Figure 4

379 & Table S3). The partial correlation of EPS, Car:Chl, sPRI, cPRI and $cPRI_{vi}$ showed that the
380 relationship between EPS and sPRI was strongly affected by the Car:Chl ratio. The Car:Chl
381 ratio had, however, considerably less effect on the relationship between cPRI, $cPRI_{vi}$ and
382 EPS (Table S6).
383

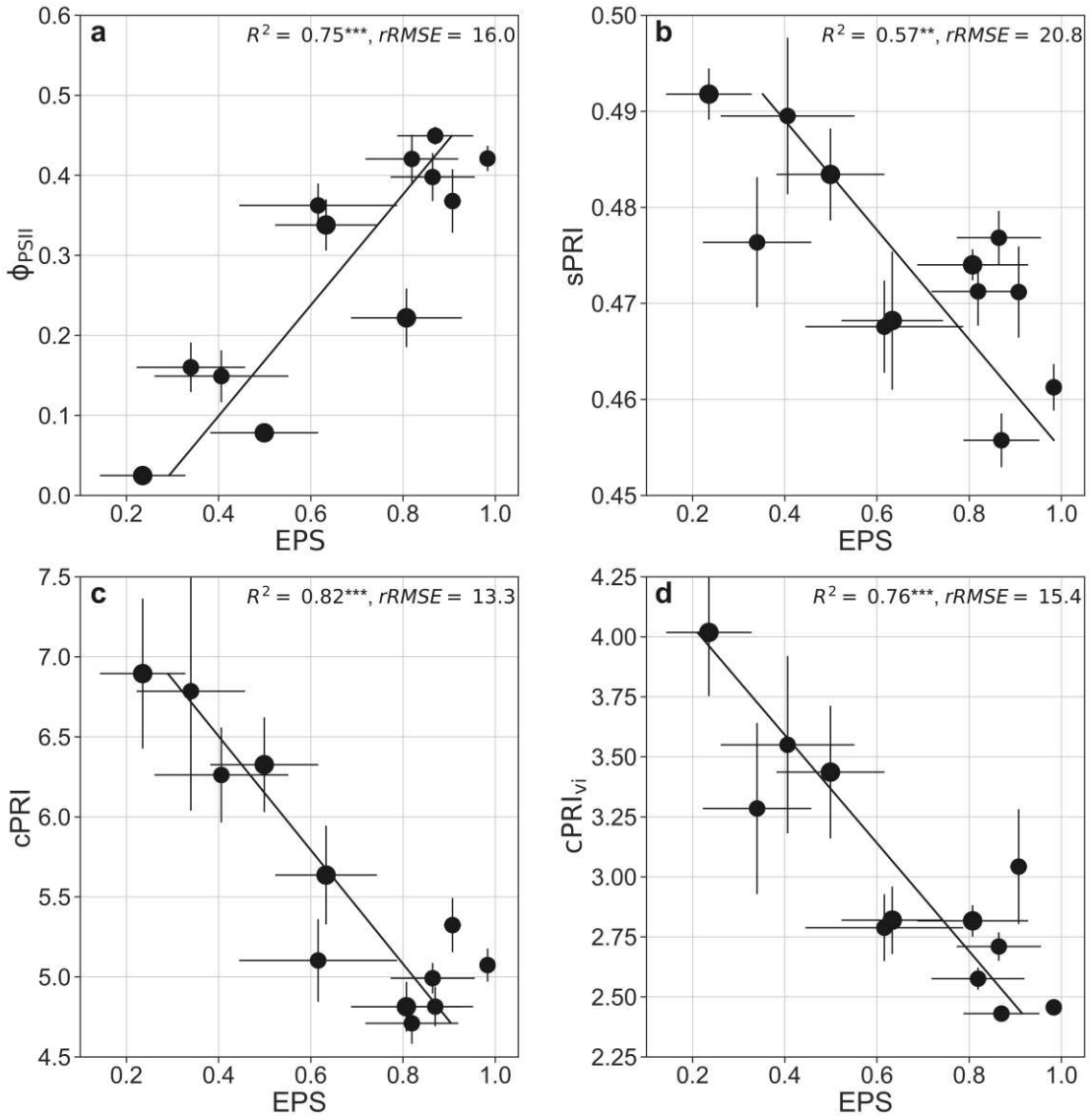

*Figure 4: (a) Relationship between epoxidation state (EPS) and photochemical yield of PSII (Φ_{PSII}). (b) Relationship between EPS and scaled photochemical reflectance index (sPRI). (c) Relationship between EPS and corrected sPRI. cPRI was calculated by normalizing the sPRI by the measured foliar pigment ratio of carotene to chlorophyll concentrations. (d) Relationship between EPS and $cPRI_{vi}$. $cPRI_{vi}$ was normalized by a vegetation index derived ratio of carotene to chlorophyll. EPS and PRI are given in arbitrary units (a.u.). The black line represents the best fitting model for all treatments for both campaigns. The asterisks indicate the significance level (** = P ≤ 0.01, *** = P ≤ 0.001). Number of samples per treatment for Campaign 1: P1 = 5, P2 = 5, P3 = 7, P4 = 5, P1S = 9, P4S = 8. Number of samples per treatment for Campaign 2: P1 = 10, P2 = 9, P3 = 10, P4 = 10, P1S = 9, P4S = 10.*

Estimation of photosynthesis by fluorescence and reflectance indices

No significant linear relationship was found between gross leaf photosynthesis (A_g) and total fluorescence (F_{tot}) along the P limitation gradient (Figure 5a), even when the highly stressed P1S treatment of the second campaign (point with lowest A_g value) is excluded. Due to the constant light conditions of the Li-6400, Φ_{PSII} showed a strong linear relationship with A_g (Figure 5b).

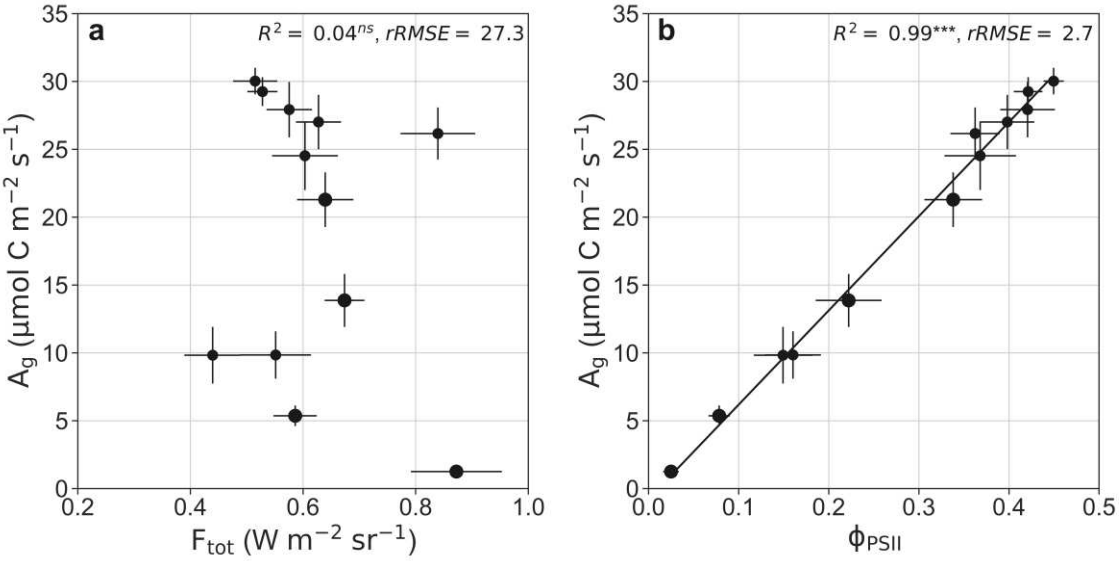

*Figure 5: a) Relationship between foliar gross photosynthesis (Ag) and total fluorescence (F_{tot}; fluorescence emitted between 650-800nm emitted from upper and lower side of the leaf). b) Relationship between foliar gross photosynthesis (A_g) and photochemical yield of PSII (Φ_{PSII}). The asterisks indicate the significance level (ns = P > 0.05, *** = P ≤ 0.001). Number of samples per treatment for Campaign 1: P1 = 5, P2 = 5, P3 = 7, P4 = 5, P1S = 9, P4S = 8. Number of samples per treatment for Campaign 2: P1 = 10, P2 = 9, P3 = 10, P4 = 10, P1S = 9, P4S = 10.*

The relationships between Φ_{PSII} and F_{yield}, as well as between $cPRI_{vi}$ and F_{yield}, were best described by a 3rd-degree polynomial (Figure 6a&b). When Φ_{PSII} was low (<0.13) and cPRI high (>3.5), F_{yield} showed the highest values (ca. 1.6 %), but decreased quickly with

increasing Φ_{PSII} and decreasing $cPRI_{vi}$. As Φ_{PSII} further increased (>0.13) and $cPRI_{vi}$ decreased (<3.5), F_{yield} increased, leading to a positive linear relationship (Figure 6a) with Φ_{PSII} and a negative linear relationship with $cPRI_{vi}$. As Φ_{PSII} exceeded 0.31 and $cPRI_{vi}$ decreased further (<2.9), F_{yield} decreased again to its lowest values (0.6%), suggesting a negative linear relationship with Φ_{PSII} and a positive relationship with $cPRI_{vi}$ (Figure 6a&b). The relationship between $cPRI_{vi}$ and Φ_{PSII} on the other hand showed a strong linear relationship (Figure 6c). We tested if a combination of $cPRI_{vi}$ and F_{yield} can improve the estimation of Φ_{PSII} (c.f. Supplementary). Even though our approach allowed the estimation of Φ_{PSII} by combining $cPRI_{vi}$ and F_{yield} it was strongly sensitive to cPRI, where a wrong classification of the stress stages (green, yellow, red, background in Figure 6a&b) lead to a strong model bias (c.f. different classification of the stress phases by cPRI in Figure S6b).

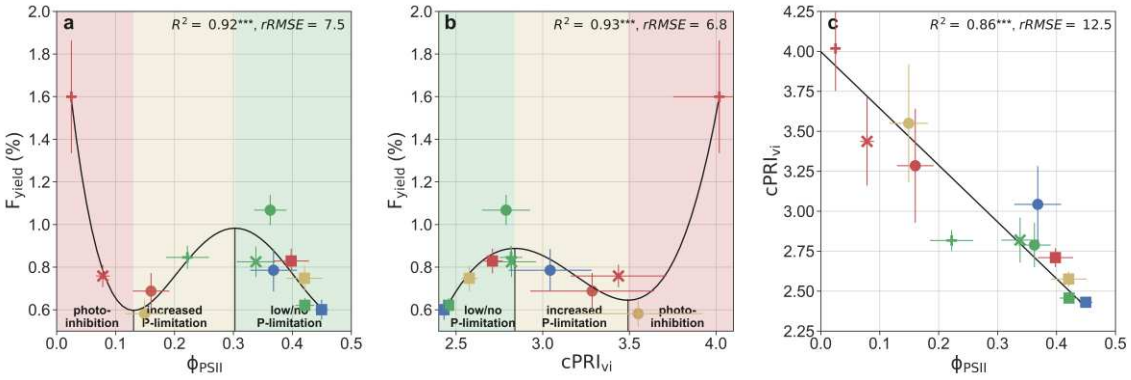

Figure 6: (a) Relationship between fluorescence yield (F_{yield}; total fluorescence emitted between 650-800nm emitted from upper and lower side of the leaf divide by absorbed photosynthetic active radiation) and photochemical yield of PSII (Φ_{PSII}). The black line represents the best fitting polynomial model for all treatments for both campaigns. The black horizontal line indicates the local minima and maxima of the polynomial model. (b) Relationship between F_{yield} and $CAR_{red\text{-}edge}$:$CI_{red\text{-}edge}$ ratio normalized scaled photochemical reflectance index ($cPRI_{vi}$). cPRI is given in arbitrary units (a.u.). The green, yellow and red background color represent the P stress level (green = low/no P stress, yellow = increased P stress, red = photoinhibition). The black line represents the best fitting polynomial model for all treatments for both

*campaigns. The black horizontal line indicates the local minima and maxima of the polynomial model. (c) Relationship between $cPRI_{vi}$ and Φ_{PSII}. Colors represent the phosphor treatments (green, P4; blue, P3; yellow, P2; red, P1), where the circles represent the first campaign and squares the second campaign. The x symbol represents treatments without arbuscular mycorrhizal fungi (AMF) of the first campaign, the plus symbol treatments without AMF of the second campaign. The asterisk indicate the significance level (** = P ≤ 0.01, *** = P ≤ 0.001). Number of samples per treatment for Campaign 1: P1 = 5, P2 = 5, P3 = 7, P4 = 5, P1S = 9, P4S = 8. Number of samples per treatment for Campaign 2: P1 = 10, P2 = 9, P3 = 10, P4 = 10, P1S = 9, P4S = 10.*

As P limitation intensified and Φ_{PSII} decreased, the $F_{\uparrow ratio}$ decreased linearly and reached its lowest point at Φ_{PSII} around 0.25. The relationship was then reversed and $F_{\uparrow ratio}$ increased with increasing Φ_{PSII} (Figure 7a). The transmittance at 685 nm (TR_{685}) decreased exponentially with increasing $CI_{red\text{-}edge}$ (R^2 = 0.94, rRMSE = 6.3%) (Figure 7b). The correction of $F_{\uparrow ratio}$ for reduced reabsorption effects under P limitation ($cF_{\uparrow ratio}$, c.f. E14) resulted in a strong linear relationship between $cF_{\uparrow ratio}$ and Φ_{PSII} (Figure 7c).

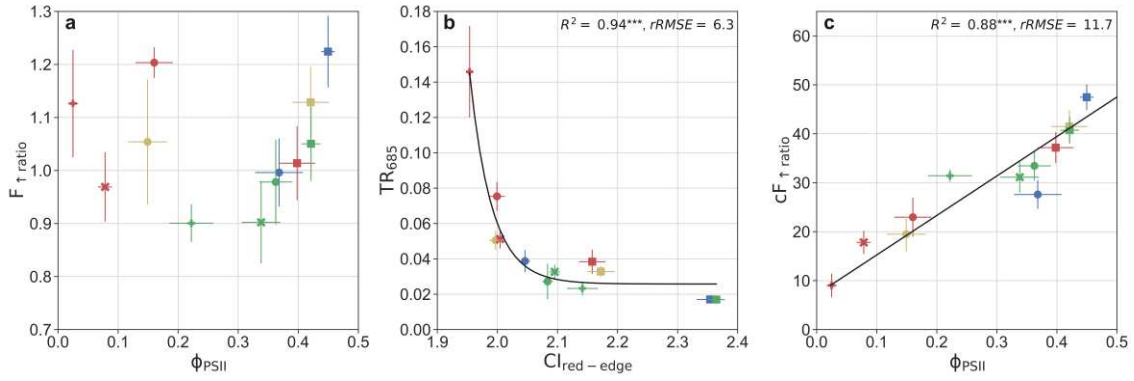

Figure 7: a) Relationship between the peak ratio of fluorescence ($F_{\uparrow ratio} = F_{\uparrow 685} / F_{\uparrow 740}$) and photochemical yield of PSII (Φ_{PSII}). The red line indicates treatments where the relationship between $F_{\uparrow ratio}$ and Φ_{PSII} is mainly driven by decreasing reabsorption effects, the dark blue line indicates treatments where their relationship between $F_{\uparrow ratio}$ and Φ_{PSII} is mainly driven by increased contribution of PSI (relative increase in $F_{\uparrow 740}$). b Relationship between the foliar transmittance at 685 nm (TR_{685}) and total Chlorophyll (Chl). The black line represents the best fitting model for all treatments for both campaigns. c) Relationship between chlorophyll normalized $F_{\uparrow ratio}$ ($cF_{\uparrow ratio}$) and Φ_{PSII}. The black line represents the best fitting model for all treatments for both campaigns. Colors represent the phosphor treatments (red: P1, yellow: P2, blue: P3, green: P4), where the circles represent the first campaign and squares the second campaign. The x symbol represent treatments without arbuscular mycorrhizal fungi (AMF) of the first campaign, the plus symbol treatments

*without AMF of the second campaign. The asterisk indicate the significance level (** = P ≤ 0.01, *** = P ≤ 0.001). Number of samples per treatment for Campaign 1: P1 = 5, P2 = 5, P3 = 7, P4 = 5, P1S = 9, P4S = 8. Number of samples per treatment for Campaign 2: P1 = 10, P2 = 9, P3 = 10, P4 = 10, P1S = 9, P4S = 10.*

The correlation of Φ_{PSII} with Chl, $CI_{red\text{-}edge}$ and $cF_{\uparrow ratio}$ showed that Φ_{PSII} correlated stronger with $cF_{\uparrow ratio}$ than with Chl or $CI_{red\text{-}edge}$. When controlled for Chl and $CI_{red\text{-}edge}$ the partial correlation of $cF_{\uparrow ratio}$ to Φ_{PSII} was still higher than the correlation between Chl and $CI_{red\text{-}edge}$ to Φ_{PSII} (Table 1). However, it has to be mentioned that the $cPRI_{vi}$ performed at a similar level than the $cF_{\uparrow ratio}$ just with an negative correlation.

*Table 1: Pearson correlation coefficient (r) of the partial correlation analysis of Φ_{PSII}, Chl, $CI_{red\text{-}edge}$, $cF_{\uparrow ratio}$ and $cPRI_{vi}$. The table shows the correlation between Φ_{PSII} and, $cF_{\uparrow ratio}$ and $cPRI_{vi}$ when controlling for their covariance with Chl and $CI_{red\text{-}edge}$. The asterisk indicate the two-tailed significance level (^{ns} = P > 0.05, * = P ≤ 0.05, ** = P ≤ 0.01, *** = P ≤ 0.001).*

		Correlation with Φ_{PSII}			
		$cF_{\uparrow ratio}$	$cPRI_{vi}$	Chl	$CI_{red\text{-}edge}$
Control variables	none	0.936***	- 0.927***	0.778**	0.782**
	Chl	0.844***	-0.807**	-	-
	$CI_{red\text{-}edge}$	0.847***	-0.800**	-	-

Discussion

Plant response to P limitation

The aim of the current study was to create different levels of P shortage, which would allow us to assess the suitability of F_{tot} as a linear predictor of leaf photosynthesis, to explore the relationship between F_{yield} and Φ_{PSII} and to test if $F_{yield,}$ the PRI, and the $F_{\uparrow ratio}$

477 are suitable predictors of Φ_{PSII} at leaf level. Detailed information about plant response to
478 P limitation of this experiment can be found in Ven *et al.* (2020).
479
480 **Implications for remote sensing of Φ_{PSII} by PRI**
481 Our results show that sPRI can be used to estimate P deficiency effects on foliar EPS
482 because of its relationship to the energy- (or pH-) dependent mechanism of non-
483 photochemical quenching. The foliar pigment content, however, exert a dominant
484 influence on the sPRI (Zhang *et al.*, 2011; Garbulsky *et al.*, 2011; Gitelson *et al.*, 2017a),
485 and therefore methods to minimize these confounding effects are needed. We were able
486 to improve the estimation of leaf-level EPS and Φ_{PSII} by normalizing the sPRI by the Car:Chl
487 ratio. We further showed that alternatively to the measured pigment pools, remotely
488 sensed indices of chlorophyll and carotenoids can be used to correct the PRI at leaf level.
489 Even though studies have generally found that PRI can be related to leaf photosynthetic
490 processes in specific ecosystems (Peñuelas *et al.*, 2011; Porcar-Castell *et al.*, 2012), a
491 universal or standardized method linking PRI to non-photochemical quenching or
492 photosynthesis at top of canopy is still lacking (Gitelson *et al.*, 2017a; Alonso *et al.*, 2017).
493
494 **Implications for remote sensing of Φ_{PSII} by SIF**
495 Results show that F_{tot} is not linearly related to leaf photosynthesis (A_g) across a P limitation
496 gradient, while the relationship of the physiologically linked parameters Φ_{PSII} and F_{yield}
497 was best described by a 3rd-degree polynomial across the P gradient. This pattern was

498 previously reported from active and passive fluorescence measurements under heat
499 stress conditions (Magney *et al.*, 2017) and active fluorescence measurements and model
500 exercises (van der Tol *et al.*, 2014). The latter have shown that F_{yield} is strongly influenced
501 by the predominant NPQ protective mechanism and that an increase in NPQ can change
502 the typically negative relationship between Φ_{PSII} and F_{yield} into a positive relationship. F_{yield}
503 can thus increase under extreme high irradiance stress conditions, or when
504 photoinhibition occurs and Φ_{PSII} is strongly downregulated while non-photochemical
505 quenching is highest (van der Tol *et al.*, 2014; Marrs *et al.*, 2020; Martini *et al.*, 2021). In
506 our experiment we observed the latter. The polynomial relationship complicates the
507 estimation of Φ_{PSII} from F_{yield}, because F_{yield} can be misinterpreted if the stress stage, and
508 consequently the corresponding relationship, is unknown. The relationship between
509 $cPRI_{vi}$ to F_{yield} is also non-monotonic, but shows opposite patterns of the relationship
510 between Φ_{PSII} to F_{yield} (Figure 6b). Even though the $cPRI_{vi}$ to F_{yield} relationship can be used
511 to detect the stress phases (c.f. Supplementary) and thereby allows the prediction of Φ_{PSII}
512 by F_{yield}, we argue that it is more straightforward to estimate Φ_{PSII} on the basis of its linear
513 relationship with $cPRI_{vi}$, particularly because the estimation of Φ_{PSII} by cPRI and F_{yield}
514 comes with a high uncertainty (c.f. Figure 6S). We show that due to its sensitivity to the
515 xanthophyll activity, cPRI and $cPRI_{vi}$ can be used to estimate Φ_{PSII} at leaf level.
516 While the breakpoint at local minima can be attributed to severe photoinhibition, the
517 light response curves indicate that the breakpoint at local maxima is caused by a switch
518 from light to P limitation due to the inhibition of ATP synthase (Carstensen *et al.*, 2018).

519 The treatment-specific light response curves shown in Figure S2, indicate that
520 observations under low P limitation (campaign 1: P3,P4 and campaign 2: P1, P2, P3, P4,
521 P4S) (Figure 6a) were light-limited during the measurements (APAR values around 450-
522 500 mmol m^{-2} s^{-1}). In contrast, the treatments with increased P limitation on the left side
523 of the local maxima (campaign 1: P1, P2, P1S, P4S and campaign 2: P1S) (Figure 6a) might
524 have been limited by inhibited ATP synthase (Figure S2).
525 These findings may also clarify why satellite and in-situ canopy measurements rarely
526 capture the right or left side of the local maxima, where F_{yield} and Φ_{PSII} share a negative
527 relationship. SIF products derived from satellite observations have a local overpass time
528 of 9:30 (GOME2) or 13:30 (OCO-2, TROPOMI). At this time of the day, and under clear sky
529 conditions (a prerequisite to obtain satellite images), photosynthesis might not be light-
530 limited, in particular during the growing season. Furthermore, satellite observations are
531 limited by their temporal and spatial resolution which complicate the detection of severe
532 stress (photoinhibition). Thus, satellite SIF products might only represent the left side of
533 the local maxima, where SIF correlates positively with photosynthesis. Even though in-
534 situ canopy measurements could theoretically track SIF under low light conditions, these
535 measurements are rare, since they are normally discarded due to increased uncertainties
536 in the retrieval of SIF under low solar angles or cloudy conditions (Meroni *et al.*, 2009).
537 Previous research showed that increasing P limitation decreases ETR of PSII more than
538 ETR of PSI (Carstensen *et al.*, 2018). This can lead to a stronger decrease in $F_{\uparrow 685}$ than in
539 $F_{\uparrow 740}$ (Buschmann, 2007). Therefore, the $F_{\uparrow ratio}$ might offer an alternative approach

allowing the estimation of photosynthetic efficiency from optical remote sensing. With increasing P limitation, however, the total chlorophyll content decreased too, resulting in an exponential increase of the transmittance at 685 nm that indicates reduced reabsorption effects on F_{685}. We assume that due to the exponential increase in transmittance, $F_{\uparrow 685}$ increases more strongly than $F_{\uparrow 740}$, resulting in an increase in the $F_{\uparrow ratio}$ with intensifying P limitation (c.f. Figure 7). Correcting $F_{\uparrow 685}$ for these effects using the exponential relationship between the transmittance at 685 nm with $CI_{red\text{-}edge}$, resulted in a strong linear relationship between $cF_{\uparrow ratio}$ and Φ_{PSII}. We thereby demonstrate that, due to the changing contribution of PSII and PSI under P limitation, the $cF_{\uparrow ratio}$ can be linked to Φ_{PSII}. At the leaf level, the $cF_{\uparrow ratio}$ was a precise and accurate predictor of Φ_{PSII}, which is of particular interest since the $cF_{\uparrow ratio}$, in contrast to F_{yield}, does not need to be normalized by APAR. Satellite based APAR depends on reflectance based estimations of fPAR, which is in particular challenging in ecosystems where the reflectance does not drop when photosynthesis is decoupled from greenness (Joiner *et al.*, 2014). Therefore the $cF_{\uparrow ratio}$ might be better suited for satellite applications than F_{yield}. At canopy level, however, the estimation of photosynthetic parameters by $cF_{\uparrow ratio}$ comes with several challenges which have to be addressed in future studies: i) the relationship of transmittance and $CI_{red\text{-}edge}$ is likely species dependent, ii) structural effects will complicate the correction for reduced reabsorption effects at canopy level (Liu & Liu, 2018; Romero *et al.*, 2020), iii) the retrieval of red SIF at canopy level comes with a lower signal quality than far-red SIF.

561 Our results are in agreement with previous studies showing that upward emitted F_{yield} can
562 contribute up to 65% to total leaf F_{yield} (Van Wittenberghe *et al.*, 2013, 2015). We also
563 showed that the contribution of $F_{\uparrow}$ to F_{tot} ($F_{\uparrow\%}$) decreased from 65% to 48% under P
564 limitation. For observations at canopy or ecosystem scale, this implies that under P limited
565 conditions an increased amount of fluorescence is emitted by the lower side of the leaf,
566 affecting the reabsorption intensity and scattering directions within the canopy. We
567 hypothesize that the changing $F_{\uparrow\%}$ under P limitation can be caused by two processes.
568 First, red fluorescence is partly reabsorbed by the foliar light harvesting complexes (Van
569 Wittenberghe *et al.*, 2015). With decreasing total chlorophyll under P limitation, more red
570 fluorescence is transmitted through the leaf, increasing red $F_{\downarrow}$ and thus decreasing $F_{\uparrow\%}$
571 (Figure S4). However, the coincident decrease of far-red $F_{\uparrow\%}$, which is less affected by
572 reabsorption and mostly scattered by internal structures of the leaf (Louis *et al.*, 2006),
573 indicates that a mechanism independent of reabsorption decreased $F_{\uparrow\%}$ under P limited
574 conditions. An alternative explanation may be related to chloroplasts moving from the
575 cell surface to the side walls of cells to protect against excessive energy, thereby
576 decreasing the fraction of light that is absorbed (Kasahara *et al.*, 2002). The chloroplast
577 avoidance movement and the subsequent realignment of the light harvesting complexes
578 may affect F emission and direction of scattering within the leaf, decreasing the fraction
579 of F escaping from the upper surface of the leaf.
580 In this study we focused on the estimation of the quantum use efficiency, an essential
581 indicator for the efficiency of the light reactions and more closely linked to fluorescence

than fluorescence is to the Calvin cycle. Further experimental work combining multiple sensors and measurement techniques at leaf and canopy are essential to better elucidate the links between fluorescence-derived remote sensing indices and photosynthesis. Such studies should address i) under which environmental conditions the relationship between F_{yield} and Φ_{PSII} changes and how relevant this might be for satellite observations; ii) if canopy F_{ratio} can be universally corrected for reabsorption effects and; iii) if this allows an improved estimation of photosynthetic activity from different sensor platforms.

Conclusion

We examined the relationship between total fluorescence and gross photosynthesis as well as the relationship between F_{yield}, F_{ratio} and the PRI to the quantum efficiency of PSII (Φ_{PSII}) along a P limitation gradient at leaf level. We demonstrate that under stable light conditions the relationship between total fluorescence and gross photosynthesis was not linear across a P gradient. We show that Φ_{PSII} cannot be predicted from F_{yield} alone due to the non-monotonic relationship between the two variables. We demonstrate, however, that the pigment corrected $cPRI_{vi}$ and $cF_{\uparrow ratio}$ share both a strong linear relationship with Φ_{PSII}, thereby enabling the estimation of Φ_{PSII} at leaf level. The advantage of one predictor over the other depends mainly on their scalability. While, the $cPRI_{vi}$ requires information about Chl:Car ratio, the $cF_{\uparrow ratio}$ depends only on Chl content, which can facilitate the upscaling.

602 The possibility to compensate for reabsorption effects at foliar level as demonstrated in
603 this study can help to improve F_{ratio} estimations. This might allow predicting light use
604 efficiency without the need of measuring green APAR. Our results imply that overlooking
605 the physiological status of vegetation may result in a misinterpretation of the SIF signal,
606 introducing errors in photosynthesis estimates. With the growing SIF research community
607 and the increasing range of applications at global scale, we would also like to stress the
608 importance of SIF measurements at leaf level. SIF measured at the leaf level will help to
609 avoid misinterpretations of canopy signals and will help to improve our understanding of
610 the changing relationships between F_{yield} and photochemical- and non-photochemical
611 quenching, under different environmental conditions.
612

613 **Acknowledgments**

614 This research was supported by the Research Foundation—Flanders (FWO) G0D5415N,
615 by the European Research Council grant ERCSyG-610028 IMBALANCE-P and by
616 Methusalem funding of the Research Council UA. Sebastian Wieneke has received funding
617 from the European Union Horizon 2020 Research and Innovation program under the
618 Marie Skłodowska-Curie grant (ReSPEc, grant no 795299). Manuela Balzarolo has received
619 funding from the European Union Horizon 2020 Research and Innovation program under
620 the Marie Skłodowska-Curie grant (INDRO, grant no 702717). Hamada AbdElgawad is a
621 postdoctoral researcher of the Research Foundation – Flanders (FWO; 12U8918N).
622

Author Contributions

SW, MB, SV designed the experiment and the research, SW, MB, AV, MSV conducted the measurements, HA, HAE performed the laboratory analysis, SV, IAJ, JP, UR, HA, HAE, MB, AV, MSV conducted review, editing and provided expert advice in different stages of the study, SV and IAJ provided funding acquisition, project administration, and resources, SW wrote the paper.

Declaration of interests

☒ The authors declare that they have no known competing financial interests or personal relationships that could have appeared to influence the work reported in this paper.

☐ The authors declare the following financial interests/personal relationships which may be considered as potential competing interests:

References

Alonso L, Van Wittenberghe S, Amorós-López J, Vila-Francés J, Gómez-Chova L, Moreno J. **2017**. Diurnal Cycle Relationships between Passive Fluorescence, PRI and NPQ of Vegetation in a Controlled Stress Experiment. *Remote Sensing* **9**: 770.

Baker NR. **2008**. Chlorophyll Fluorescence: A Probe of Photosynthesis In Vivo. *Annual Review of Plant Biology* **59**: 89–113.

Balzarolo M, Peñuelas J, Filella I, Portillo-Estrada M, Ceulemans R. **2018**. Assessing Ecosystem Isoprene Emissions by Hyperspectral Remote Sensing. *Remote Sensing* **10**: 1086.

Buschmann C. **2007**. Variability and application of the chlorophyll fluorescence emission ratio red/far-red of leaves. *Photosynthesis Research* **92**: 261–271.

Carstensen A, Herdean A, Schmidt SB, Sharma A, Spetea C, Pribil M, Husted S. **2018**. The impacts of phosphorus deficiency on the photosynthetic electron transport chain. *Plant Physiology*: pp.01624.2017.

Ciais P, Sabine C, Bala G, Bopp L, Brovkin V, Canadell J, Chhabra A, DeFries R, Galloway J, Heimann M, *et al.* 2014. Carbon and other biogeochemical cycles. In: Climate change 2013: the physical science basis. Contribution of Working Group I to the Fifth Assessment Report of the Intergovernmental Panel on Climate Change. Cambridge University Press, 465–570.

Conroy JP, Smillie RM, Küppers M, Bevege DI, Barlow EW. **1986**. Chlorophyll a Fluorescence and Photosynthetic and Growth Responses of Pinus radiata to Phosphorus Deficiency, Drought Stress, and High CO2. *Plant Physiology* **81**: 423–429.

Cui T, Sun R, Qiao C, Zhang Q, Yu T, Liu G, Liu Z. **2017**. Estimating Diurnal Courses of Gross Primary Production for Maize: A Comparison of Sun-Induced Chlorophyll Fluorescence, Light-Use Efficiency and Process-Based Models. *Remote Sensing* **9**: 1267.

Daszkowska-Golec A, Szarejko I. **2013**. Open or Close the Gate – Stomata Action Under the Control of Phytohormones in Drought Stress Conditions. *Frontiers in Plant Science* **4**.

Dechant B, Ryu Y, Badgley G, Zeng Y, Berry JA, Zhang Y, Goulas Y, Li Z, Zhang Q, Kang M, *et al.* 2020. Canopy structure explains the relationship between photosynthesis and sun-induced chlorophyll fluorescence in crops. *Remote Sensing of Environment* **241**: 111733.

Filella I, Porcar-Castell A, Munné-Bosch S, Bäck J, Garbulsky MF, Peñuelas J. **2009**. PRI assessment of long-term changes in carotenoids/chlorophyll ratio and short-term changes in de-epoxidation state of the xanthophyll cycle. *International Journal of Remote Sensing* **30**: 4443–4455.

Foley S, Rivard B, Sanchez-Azofeifa GA, Calvo J. **2006**. Foliar spectral properties following leaf clipping and implications for handling techniques. *Remote Sensing of Environment* **103**: 265–275.

Frankenberg C, Fisher JB, Worden J, Badgley G, Saatchi SS, Lee J-E, Toon GC, Butz A, Jung M, Kuze A, *et al.* 2011. New global observations of the terrestrial carbon cycle from GOSAT: Patterns of plant fluorescence with gross primary productivity. *Geophysical Research Letters* **38**: L17706.

Frydenvang J, Maarschalkerweerd M van, Carstensen A, Mundus S, Schmidt SB, Pedas PR, Laursen KH, Schjoerring JK, Husted S. **2015**. Sensitive Detection of Phosphorus Deficiency in Plants Using Chlorophyll a Fluorescence. *Plant Physiology* **169**: 353–361.

Gamon JA, Field CB, Fredeen AL, Thayer S. **2001**. Assessing photosynthetic downregulation in sunflower stands with an optically-based model. *Photosynthesis Research* **67**: 113–125.

Gamon JA, Peñuelas J, Field CB. **1992**. A narrow-waveband spectral index that tracks diurnal changes in photosynthetic efficiency. *Remote Sensing of Environment* **41**: 35–44.

Garbulsky MF, Peñuelas J, Gamon J, Inoue Y, Filella I. **2011**. The photochemical reflectance index (PRI) and the remote sensing of leaf, canopy and ecosystem radiation use efficiencies: A review and meta-analysis. *Remote Sensing of Environment* **115**: 281–297.

Ge Z, Rubio G, Lynch JP. **2000**. The importance of root gravitropism for inter-root competition and phosphorus acquisition efficiency: results from a geometric simulation model. *Plant and Soil* **218**: 159–171.

Genty B, Briantais J-M, Baker NR. **1989**. The relationship between the quantum yield of photosynthetic electron transport and quenching of chlorophyll fluorescence. *Biochimica et Biophysica Acta (BBA) - General Subjects* **990**: 87–92.

Giovannetti M, Mosse B. **1980**. An Evaluation of Techniques for Measuring Vesicular Arbuscular Mycorrhizal Infection in Roots. *New Phytologist* **84**: 489–500.

Gitelson A. **2020**. Towards a generic approach to remote non-invasive estimation of foliar carotenoid-to-chlorophyll ratio. *Journal of Plant Physiology* **252**: 153227.

Gitelson AA, Gamon JA, Solovchenko A. **2017a**. Multiple drivers of seasonal change in PRI: Implications for photosynthesis 2. Stand level. *Remote Sensing of Environment* **190**: 198–206.

Gitelson AA, Gamon JA, Solovchenko A. **2017b**. Multiple drivers of seasonal change in PRI: Implications for photosynthesis 1. Leaf level. *Remote Sensing of Environment* **191**: 110–116.

Gitelson AA, Gritz † Y, Merzlyak MN. **2003**. Relationships between leaf chlorophyll content and spectral reflectance and algorithms for non-destructive chlorophyll assessment in higher plant leaves. *Journal of Plant Physiology* **160**: 271–282.

Gitelson AA, Keydan GP, Merzlyak MN. **2006**. Three-band model for noninvasive estimation of chlorophyll, carotenoids, and anthocyanin contents in higher plant leaves. *Geophysical Research Letters* **33**.

Guanter L, Zhang Y, Jung M, Joiner J, Voigt M, Berry JA, Frankenberg C, Huete AR, Zarco-Tejada P, Lee J-E, *et al.* 2014. Global and time-resolved monitoring of crop photosynthesis with chlorophyll fluorescence. *Proceedings of the National Academy of Sciences* **111**: E1327–E1333.

Harris CR, Millman KJ, van der Walt SJ, Gommers R, Virtanen P, Cournapeau D, Wieser E, Taylor J, Berg S, Smith NJ, *et al.* 2020. Array programming with NumPy. *Nature* **585**: 357–362.

Hou E, Wen D, Jiang L, Luo X, Kuang Y, Lu X, Chen C, Allen KT, He X, Huang X, *et al.* 2021. Latitudinal patterns of terrestrial phosphorus limitation over the globe. *Ecology Letters* **24**: 1420–1431.

Joiner J, Yoshida Y, Vasilkov AP, Schaefer K, Jung M, Guanter L, Zhang Y, Garrity S, Middleton EM, Huemmrich KF, *et al.* 2014. The seasonal cycle of satellite chlorophyll fluorescence observations and its relationship to vegetation phenology and ecosystem atmosphere carbon exchange. *Remote Sensing of Environment* **152**: 375–391.

Kasahara M, Kagawa T, Oikawa K, Suetsugu N, Miyao M, Wada M. **2002**. Chloroplast avoidance movement reduces photodamage in plants. *Nature* **420**: 829.

Kohzuma K, Hikosaka K. **2018**. Physiological validation of photochemical reflectance index (PRI) as a photosynthetic parameter using Arabidopsis thaliana mutants. *Biochemical and Biophysical Research Communications* **498**: 52–57.

Le A, S T, Je O, Kk T. **2011**. *Stomatal Responses to Drought Stress and Air Humidity*. IntechOpen.

Liao H, Rubio G, Yan X, Cao A, Brown KM, Lynch JP. **2001**. Effect of phosphorus availability on basal root shallowness in common bean. *Plant and Soil* **232**: 69–79.

Lichtenthaler HK, Rinderle U. **1988**. The Role of Chlorophyll Fluorescence in The Detection of Stress Conditions in Plants. *C R C Critical Reviews in Analytical Chemistry* **19**: S29–S85.

Lima JD, Mosquim PR, Da Matta FM. **1999**. Leaf Gas Exchange and Chlorophyll Fluorescence Parameters in Phaseolus Vulgaris as Affected by Nitrogen and Phosphorus Deficiency. *Photosynthetica* **37**: 113–121.

Liu X, Liu L. **2018**. Influence of the canopy BRDF characteristics and illumination conditions on the retrieval of solar-induced chlorophyll fluorescence. *International Journal of Remote Sensing* **39**: 1782–1799.

Louis J, Cerovic ZG, Moya I. **2006**. Quantitative study of fluorescence excitation and emission spectra of bean leaves. *Journal of Photochemistry and Photobiology B: Biology* **85**: 65–71.

Magney TS, Barnes ML, Yang X. **2020**. On the Covariation of Chlorophyll Fluorescence and Photosynthesis Across Scales. *Geophysical Research Letters* **47**: e2020GL091098.

Magney TS, Bowling DR, Logan BA, Grossmann K, Stutz J, Blanken PD, Burns SP, Cheng R, Garcia MA, Köhler P, *et al.* 2019. Mechanistic evidence for tracking the seasonality of

photosynthesis with solar-induced fluorescence. *Proceedings of the National Academy of Sciences* **116**: 11640–11645.

Magney Troy S., Frankenberg Christian, Fisher Joshua B., Sun Ying, North Gretchen B., Davis Thomas S., Kornfeld Ari, Siebke Katharina. **2017**. Connecting active to passive fluorescence with photosynthesis: a method for evaluating remote sensing measurements of Chl fluorescence. *New Phytologist* **215**: 1594–1608.

Maguire AJ, Eitel JUH, Griffin KL, Magney TS, Long RA, Vierling LA, Schmiege SC, Jennewein JS, Weygint WA, Boelman NT, *et al.* 2020. On the Functional Relationship Between Fluorescence and Photochemical Yields in Complex Evergreen Needleleaf Canopies. *Geophysical Research Letters* **47**: e2020GL087858.

Marrs JK, Reblin JS, Logan BA, Allen DW, Reinmann AB, Bombard DM, Tabachnik D, Hutyra LR. **2020**. Solar-Induced Fluorescence Does Not Track Photosynthetic Carbon Assimilation Following Induced Stomatal Closure. *Geophysical Research Letters* **47**: e2020GL087956.

Marschner H, Römheld V, Horst WJ, Martin P. **1986**. Root-induced changes in the rhizosphere: Importance for the mineral nutrition of plants. *Zeitschrift für Pflanzenernährung und Bodenkunde* **149**: 441–456.

Martini D, Sakowska K, Wohlfahrt G, Pacheco-Labrador J, van der Tol C, Porcar-Castell A, Magney TS, Carrara A, Colombo R, El-Madany TS, *et al.* 2021. Heatwave breaks down the linearity between sun-induced fluorescence and gross primary production. *New Phytologist* **n/a**.

Maxwell K, Johnson GN. **2000**. Chlorophyll fluorescence—a practical guide. *Journal of Experimental Botany* **51**: 659–668.

McKinney W. **2010**. Data Structures for Statistical Computing in Python. *Proceedings of the 9th Python in Science Conference*: 56–61.

Meroni M, Rossini M, Guanter L, Alonso L, Rascher U, Colombo R, Moreno J. **2009**. Remote sensing of solar-induced chlorophyll fluorescence: Review of methods and applications. *Remote Sensing of Environment* **113**: 2037–2051.

Merzlyak MN, Gitelson AA, Chivkunova OB, Rakitin VY. **1999**. Non-destructive optical detection of pigment changes during leaf senescence and fruit ripening. *Physiologia Plantarum* **106**: 135–141.

Miao G, Kaiyu G, Xi Y, J. BC, A. BJ, H. DE, Jin W, E. MC, Katherine M, Yaping C, *et al.* 2018. Sun-Induced Chlorophyll Fluorescence, Photosynthesis, and Light Use Efficiency of a Soybean Field from Seasonally Continuous Measurements. *Journal of Geophysical Research: Biogeosciences* **123**: 610–623.

Migliavacca M, Perez-Priego O, Rossini M, El-Madany TS, Moreno G, van der Tol C, Rascher U, Berninger A, Bessenbacher V, Burkart A, *et al.* 2017. Plant functional traits and canopy structure control the relationship between photosynthetic CO2 uptake and far-red sun-induced

776 fluorescence in a Mediterranean grassland under different nutrient availability. *New Phytologist*:
777 n/a-n/a.

778 **Mohammed GH, Colombo R, Middleton EM, Rascher U, van der Tol C, Nedbal L, Goulas Y,**
779 **Pérez-Priego O, Damm A, Meroni M, *et al.* 2019**. Remote sensing of solar-induced chlorophyll
780 fluorescence (SIF) in vegetation: 50 years of progress. *Remote Sensing of Environment* **231**:
781 111177.

782 **Müller P, Li X-P, Niyogi KK**. **2001**. Non-Photochemical Quenching. A Response to Excess Light
783 Energy. *Plant Physiology* **125**: 1558–1566.

784 **Pedregosa F, Varoquaux G, Gramfort A, Michel V, Thirion B, Grisel O, Blondel M, Prettenhofer**
785 **P, Weiss R, Dubourg V, *et al.* 2011**. Scikit-learn: Machine Learning in Python. *Journal of Machine*
786 *Learning Research* **12**: 2825–2830.

787 **Penuelas J, Baret F, Filella I**. **1995**. Semi-empirical indices to assess carotenoids/chlorophyll a
788 ratio from leaf spectral reflectance. *Photosynthetica* **31**: 221–230.

789 **Peñuelas J, Filella I, Gamon JA**. **1995**. Assessment of photosynthetic radiation-use efficiency
790 with spectral reflectance. *New Phytologist* **131**: 291–296.

791 **Peñuelas J, Filella I, Gamon JA, Field C**. **1997**. Assessing photosynthetic radiation-use efficiency
792 of emergent aquatic vegetation from spectral reflectance. *Aquatic Botany* **58**: 307–315.

793 **Peñuelas J, Gamon JA, Fredeen AL, Merino J, Field CB**. **1994**. Reflectance indices associated
794 with physiological changes in nitrogen- and water-limited sunflower leaves. *Remote Sensing of*
795 *Environment* **48**: 135–146.

796 **Peñuelas J, Garbulsky MF, Filella I**. **2011**. Photochemical reflectance index (PRI) and remote
797 sensing of plant CO2 uptake. *New Phytologist* **191**: 596–599.

798 **Pinto F, Damm A, Schickling A, Panigada C, Cogliati S, Müller-Linow M, Balvora A, Rascher U**.
799 **2016**. Sun-induced chlorophyll fluorescence from high-resolution imaging spectroscopy data to
800 quantify spatio-temporal patterns of photosynthetic function in crop canopies. *Plant, Cell &*
801 *Environment* **39**: 1500–1512.

802 **Porcar-Castell A, Garcia-Plazaola JI, Nichol CJ, Kolari P, Olascoaga B, Kuusinen N, Fernández-**
803 **Marín B, Pulkkinen M, Juurola E, Nikinmaa E**. **2012**. Physiology of the seasonal relationship
804 between the photochemical reflectance index and photosynthetic light use efficiency. *Oecologia*
805 **170**: 313–323.

806 **Porcar-Castell A, Tyystjärvi E, Atherton J, Tol C van der, Flexas J, Pfündel EE, Moreno J,**
807 **Frankenberg C, Berry JA**. **2014**. Linking chlorophyll a fluorescence to photosynthesis for remote
808 sensing applications: mechanisms and challenges. *Journal of Experimental Botany*: eru191.

809 **Rahimzadeh-Bajgiran P, Munehiro M, Omasa K**. **2012**. Relationships between the
810 photochemical reflectance index (PRI) and chlorophyll fluorescence parameters and plant
811 pigment indices at different leaf growth stages. *Photosynthesis Research* **113**: 261–271.

Rahman AF, Cordova VD, Gamon JA, Schmid HP, Sims DA. **2004**. Potential of MODIS ocean bands for estimating CO2 flux from terrestrial vegetation: A novel approach. *Geophysical Research Letters* **31**.

Rajewicz PA, Atherton J, Alonso L, Porcar-Castell A. **2019**. Leaf-Level Spectral Fluorescence Measurements: Comparing Methodologies for Broadleaves and Needles. *Remote Sensing* **11**: 532.

Romero JM, Cordon GB, Lagorio MG. **2020**. Re-absorption and scattering of chlorophyll fluorescence in canopies: A revised approach. *Remote Sensing of Environment* **246**: 111860.

Sims DA, Gamon JA. **2002**. Relationships between leaf pigment content and spectral reflectance across a wide range of species, leaf structures and developmental stages. *Remote Sensing of Environment* **81**: 337–354.

Sun Y, Frankenberg C, Jung M, Joiner J, Guanter L, Köhler P, Magney T. **2018**. Overview of Solar-Induced chlorophyll Fluorescence (SIF) from the Orbiting Carbon Observatory-2: Retrieval, cross-mission comparison, and global monitoring for GPP. *Remote Sensing of Environment*.

Thayer SS, Björkman O. **1990**. Leaf Xanthophyll content and composition in sun and shade determined by HPLC. *Photosynthesis Research* **23**: 331–343.

van der Tol C, Berry JA, Campbell PKE, Rascher U. **2014**. Models of fluorescence and photosynthesis for interpreting measurements of solar induced chlorophyll fluorescence. *Journal of Geophysical Research: Biogeosciences*: 2014JG002713.

Van Wittenberghe S, Alonso L, Verrelst J, Hermans I, Delegido J, Veroustraete F, Valcke R, Moreno J, Samson R. **2013**. Upward and downward solar-induced chlorophyll fluorescence yield indices of four tree species as indicators of traffic pollution in Valencia. *Environmental Pollution* **173**: 29–37.

Van Wittenberghe S, Alonso L, Verrelst J, Moreno J, Samson R. **2015**. Bidirectional sun-induced chlorophyll fluorescence emission is influenced by leaf structure and light scattering properties — A bottom-up approach. *Remote Sensing of Environment* **158**: 169–179.

Ven A, Verlinden MS, Fransen E, Olsson PA, Verbruggen E, Wallander H, Vicca S. **2020**. Phosphorus addition increased carbon partitioning to autotrophic respiration but not to biomass production in an experiment with Zea mays. *Plant, Cell & Environment* **43**: 2054–2065.

Verlinden MS, Ven A, Verbruggen E, Janssens IA, Wallander H, Vicca S. **2018**. Favorable effect of mycorrhizae on biomass production efficiency exceeds their carbon cost in a fertilization experiment. *Ecology* **99**: 2525–2534.

Vicca S, Balzarolo M, Filella I, Granier A, Herbst M, Knohl A, Longdoz B, Mund M, Nagy Z, Pintér K, *et al.* 2016. Remotely-sensed detection of effects of extreme droughts on gross primary production. *Scientific Reports* **6**: 28269.

Vierheilig H, Schweiger P, Brundrett M. **2005**. An overview of methods for the detection and observation of arbuscular mycorrhizal fungi in roots†. *Physiologia Plantarum* **125**: 393–404.

Virtanen P, Gommers R, Oliphant TE, Haberland M, Reddy T, Cournapeau D, Burovski E, Peterson P, Weckesser W, Bright J, *et al.* 2020. SciPy 1.0: fundamental algorithms for scientific computing in Python. *Nature Methods* **17**: 261–272.

Wieneke S, Burkart A, Cendrero-Mateo MP, Julitta T, Rossini M, Schickling A, Schmidt M, Rascher U. **2018**. Linking photosynthesis and sun-induced fluorescence at sub-daily to seasonal scales. *Remote Sensing of Environment* **219**: 247–258.

Wong CYS, Gamon JA. **2015**. Three causes of variation in the photochemical reflectance index (PRI) in evergreen conifers. *New Phytologist* **206**: 187–195.

Wood JD, Griffis TJ, Baker JM, Frankenberg C, Verma M, Yuen K. **2017**. Multiscale analyses of solar-induced florescence and gross primary production. *Geophysical Research Letters* **44**: 2016GL070775.

Woodgate W, Suarez L, van Gorsel E, Cernusak LA, Dempsey R, Devilla R, Held A, Hill MJ, Norton AJ. **2019**. tri-PRI: A three band reflectance index tracking dynamic photoprotective mechanisms in a mature eucalypt forest. *Agricultural and Forest Meteorology* **272–273**: 187–201.

Yang K, Ryu Y, Dechant B, Berry JA, Hwang Y, Jiang C, Kang M, Kim J, Kimm H, Kornfeld A, *et al.* 2018. Sun-induced chlorophyll fluorescence is more strongly related to absorbed light than to photosynthesis at half-hourly resolution in a rice paddy. *Remote Sensing of Environment* **216**: 658–673.

Yang X, Tang J, Mustard JF, Lee J-E, Rossini M, Joiner J, Munger JW, Kornfeld A, Richardson AD. **2015**. Solar-induced chlorophyll fluorescence that correlates with canopy photosynthesis on diurnal and seasonal scales in a temperate deciduous forest. *Geophysical Research Letters* **42**: 2015GL063201.

Yaryura P, Cordon G, Leon M, Kerber N, Pucheu N, Rubio G, García A, Lagorio MG. **2009**. Effect of Phosphorus Deficiency on Reflectance and Chlorophyll Fluorescence of Cotyledons of Oilseed Rape (Brassica napus L.). *Journal of Agronomy and Crop Science* **195**: 186–196.

Zhang C, Filella I, Liu D, Ogaya R, Llusià J, Asensio D, Peñuelas J. **2017**. Photochemical Reflectance Index (PRI) for Detecting Responses of Diurnal and Seasonal Photosynthetic Activity to Experimental Drought and Warming in a Mediterranean Shrubland. *Remote Sensing* **9**: 1189.

Zhang Q, Wang YP, Pitman AJ, Dai YJ. **2011**. Limitations of nitrogen and phosphorous on the terrestrial carbon uptake in the 20th century. *Geophysical Research Letters* **38**: L22701.

Zhang Y, Xiao X, Jin C, Dong J, Zhou S, Wagle P, Joiner J, Guanter L, Zhang Y, Zhang G, *et al.* 2016. Consistency between sun-induced chlorophyll fluorescence and gross primary production of vegetation in North America. *Remote Sensing of Environment* **183**: 154–169.

Zhou X, Huang W, Kong W, Ye H, Dong Y, Casa R. **2017**. Assessment of leaf carotenoids content with a new carotenoid index: Development and validation on experimental and model data. *International Journal of Applied Earth Observation and Geoinformation* **57**: 24–35.

Zhou X, Huang W, Zhang J, Kong W, Casa R, Huang Y. **2019**. A novel combined spectral index for estimating the ratio of carotenoid to chlorophyll content to monitor crop physiological and phenological status. *International Journal of Applied Earth Observation and Geoinformation* **76**: 128–142.

Supplementary data

Mycorrhizal colonization

In both campaigns, mycorrhizal colonization in roots was verified in July and August by sampling roots from two plants per mesocosm. Per plant, 20 cm of one lateral root containing root hair was excavated, cut and stored at 5 °C for maximum two days. These roots were cleared and stained using a non-vital staining technique (as described by Vierheilig et al., 2005), using a 5% KOH-solution and a Sheaffer Black Ink solution (10% ink in a 10% acetic acid solution). The roots were transferred to a microscope slide and mycorrhizal colonization was quantified by counting arbuscules, vesicles and hyphae applying the gridline intersection method (Giovannetti & Mosse, 1980; Vierheilig *et al.*, 2005) (Figure S1a).

Table S1: Average (mean) and standard error (SE) of mycorrhizal colonization in roots, expressed as % of roots colonized by hyphae, arbuscules or vesicules for each treatment one and two months after planting.

mycorrhizal colonization in roots

treatment	*hyphae*		*arbuscules*		*vesicles*	
	%		*%*		*%*	
	one month after planting					
	mean	*se*	*mean*	*se*	*mean*	*se*
P1	18.6	3.8	2.4	0.8	2	1.2
P2	13.4	4.3	2.4	1.5	1	0.6
P3	33.6	6.7	11.8	3.6	5.8	2.1
P4	28.5	7.3	11.1	3.9	5.2	2
P1_noAMF	0	0	0	0	0	0
P4_noAMF	0	0	0	0	0	0
P-fertilization effect	NA		NA		NA	
P-fertilization effect	p = 0.18		p = 0.14		p = 0.23	
	two months after planting					
	mean	*se*	*mean*	*se*	*mean*	*se*
P1	50.4	6.6	11.6	3.1	20	6.2
P2	35.6	11.1	7.2	3.7	11.6	5.5
P3	53.2	5.2	9.2	2.4	14	2.2
P4	63.7	9	22.1	5.8	28.5	7
P1_noAMF	0	0	0	0	0	0
P4_noAMF	0	0	0	0	0	0
P-fertilization effect	p < 0.01		p < 0.01		p < 0.01	
P-fertilization effect	p = 0.08		p = 0.03		p = 0.13	

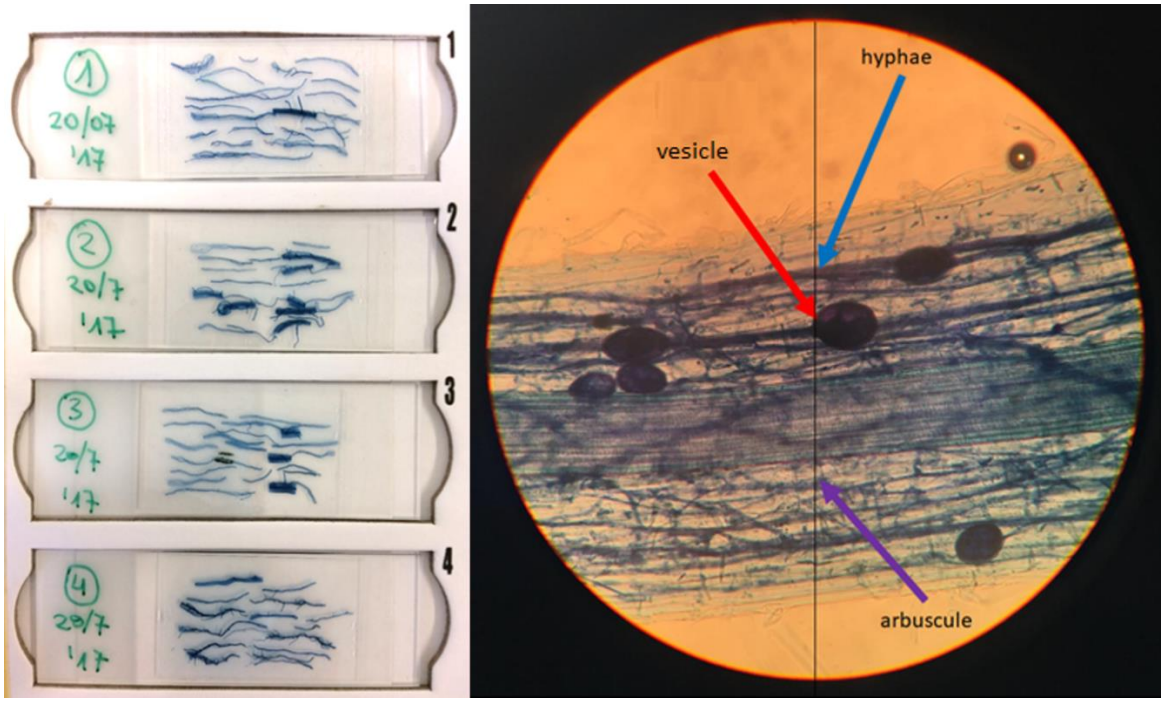

Figure S1: (left) Four microscope slides with root pieces. (right) A microscope view on a stained maize root containing a lot of AMF arbuscules, vesicles and hyphae. Each arrow goes to the first of a kind of AMF structure crossing the gridline (from above to below).

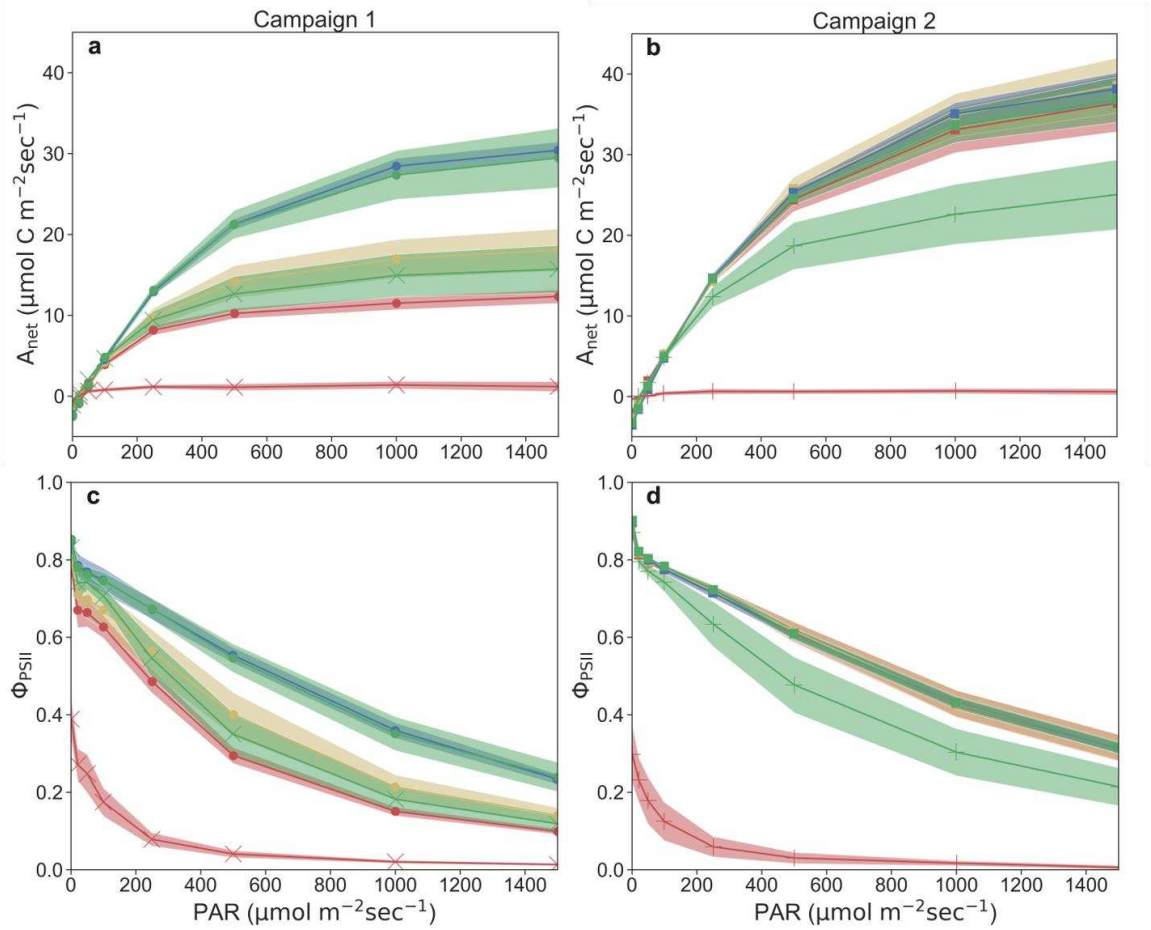

910

911 Figure S2: Averaged light response curves of five leaves and six different treatments measured during
912 campaign one (a) and campaign two (b). Shaded colors represent the standard deviation of the five leaves.
913 Dot colors represent the treatments (green, P4; blue, P3; yellow, P2; red, P1), and the crosses represent the
914 treatments without arbuscular mycorrhizal fungi (P4S, P1S). P1, P2, P3 and P4 indicate treatment with 2.5,
915 5, 10 and 20 kg P ha^{-1} triple superphosphate, respectively. P1S and P4S were pasteurized to ensure the
916 absence of arbuscular mycorrhizal fungi.

917

Composition of foliar pigments under P limitation

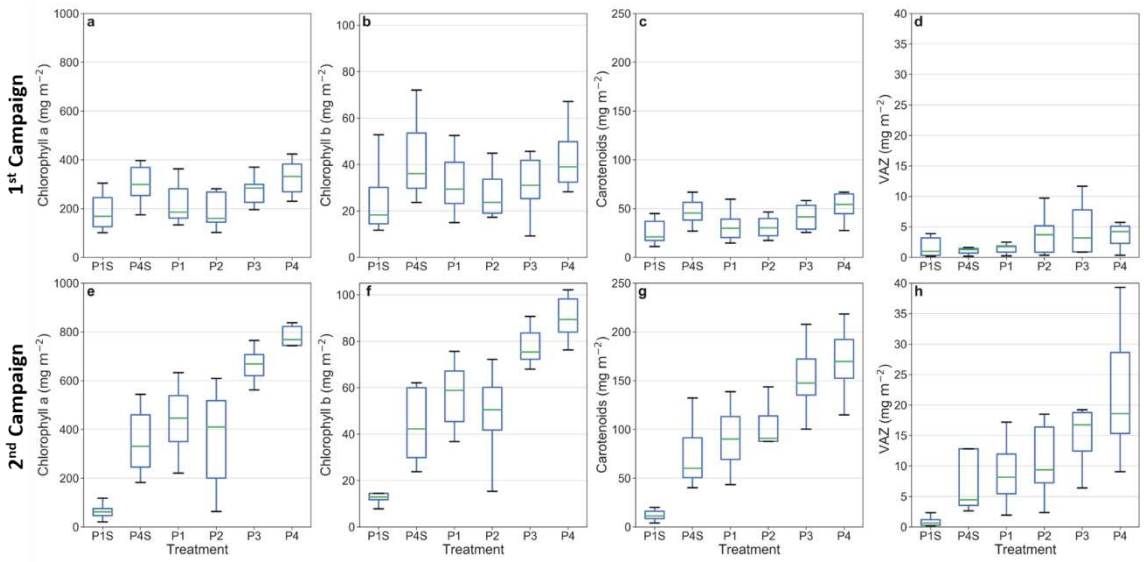

Figure S3: Box plots of chlorophyll a , chlorophyll b, carotenoids and the total xanthophyll pigment (VAZ) content 27-29 days after seeding (DAS, first campaign) a-d, and 57-61 DAS (second campaign) e-h. P1, P2, P3 and P4 indicate treatment with 2.5, 5, 10 and 20 kg P ha^{-1} triple superphosphate, respectively. P1S and P4S were pasteurized to ensure the absence of arbuscular mycorrhizal fungi.

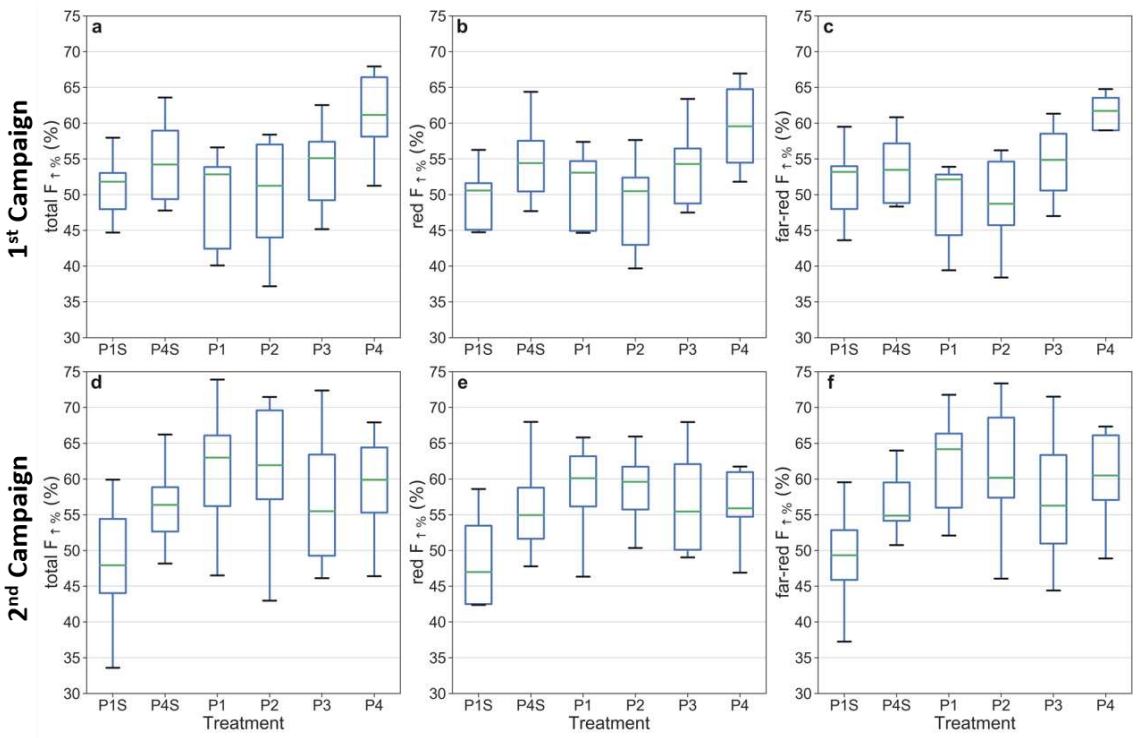

924

925 *Figure S4: Box plots of the contribution of upward emitted red , far-red and total fluorescence (F↑%). a, b &*

926 *c 27-29 days after seeding (first campaign), d, e & f 57-61 days after seeding (second campaign). P1, P2, P3*

927 *and P4 indicate treatment with 2.5, 5, 10 and 20 kg P ha^{-1} triple superphosphate, respectively. P1S and P4S*

928 *were pasteurized to ensure the absence of arbuscular mycorrhizal fungi.*

929

Table S2: P-values of the two-sided t-test for the differences in total chlorophyll content (Chl), the ratio between carotenoids and total chlorophyll (Car:Chl), the ratio of the total xanthophyll pigment content to total chlorophyll (VAZ:Chl) and the epoxidation state (EPS) 27-29 days after seeding (Campaign 1), and 57-61 days after seeding (Campaign 2). P1, P2, P3 and P4 indicate treatment with 2.5, 5, 10 and 20 kg P ha^{-1} triple superphosphate, respectively. P1S and P4S were pasteurized to ensure the absence of arbuscular mycorrhizal fungi.

	Campaign 1																			
	Chl					Car : Chl					VAZ : Chl					VAZ : Chl				
	P1S	P4S	P1	P2	P3	P1S	P4S	P1	P2	P3	P1S	P4S	P1	P2	P3	P1S	P4S	P1	P2	P3
P4S	0.020	-	-	-	-	0.823	-	-	-	-	0.237	-	-	-	-	0.423	-	-	-	-
P1	0.372	0.114	-	-	-	0.428	0.105	-	-	-	0.359	0.246	-	-	-	0.357	0.094	-	-	-
P2	0.794	0.037	0.519	-	-	0.647	0.322	0.111	-	-	0.439	0.036	0.062	-	-	0.623	0.237	0.729	-	-
P3	0.135	0.250	0.562	0.214	-	0.607	0.404	0.198	0.89	-	0.351	0.107	0.14	0.702	-	0.007	0.031	5E-04	0.005	-
P4	0.004	0.958	0.044	0.007	0.131	0.963	0.47	0.078	0.542	0.559	0.769	0.017	0.09	0.2	0.251	0.574	0.934	0.208	0.368	0.116
	Campaign 2																			
	Chl					Car : Chl					VAZ : Chl					VAZ : Chl				
	P1S	P4S	P1	P2	P3	P1S	P4S	P1	P2	P3	P1S	P4S	P1	P2	P3	P1S	P4S	P1	P2	P3
P4S	0.001	-	-	-	-	0.060	-	-	-	-	0.142	-	-	-	-	0.001	-	-	-	-
P1	0.001	0.728	-	-	-	0.063	0.425	-	-	-	0.309	0.274	-	-	-	0.001	0.708	-	-	-
P2	0.001	0.944	0.579	-	-	0.027	0.752	0.201	-	-	0.038	0.624	0.073	-	-	0.001	0.941	0.743	-	-
P3	0.001	0.007	0.001	0.001	-	0.006	0.291	0.034	0.419	-	0.059	0.558	0.110	0.875	-	0.001	0.669	0.965	0.702	-
P4	0.001	0.001	0.001	0.001	0.051	0.006	0.383	0.032	0.575	0.723	0.042	0.878	0.093	0.669	0.590	0.001	0.142	0.211	0.122	0.188

Table S3: P-values of the two-sided t-test for the differences in gross photosynthesis (Ag), quantum efficiency of PSII (ΦPSII)), ratio of Ag to dark respiration (Rd) and the fraction of absorbed photochemical active radiation (fPAR), 27-29 days after seeding (Campaign 1), and 57-61 days after seeding (Campaign 2). P1, P2, P3 and P4 indicate treatment with 2.5, 5, 10 and 20 kg P ha-1 triple superphosphate, respectively. P1S and P4S were pasteurized to ensure the absence of arbuscular mycorrhizal fungi.

	Campaign 1																			
	A_g					Φ_{PSII}					A_g/R_d					fPAR				
	P1S	P4S	P1	P2	P3	P1S	P4S	P1	P2	P3	P1S	P4S	P1	P2	P3	P1S	P4S	P1	P2	P3
P4S	0.001	-	-	-	-	0.000	-	-	-	-	0.020	-	-	-	-	0.804	-	-	-	-
P1	0.030	0.001	-	-	-	0.024	0.001	-	-	-	0.405	0.043	-	-	-	0.908	0.770	-	-	-
P2	0.052	0.001	0.995	-	-	0.048	0.001	0.808	-	-	0.269	0.231	0.604	-	-	0.172	0.189	0.314	-	-
P3	0.001	0.327	0.001	0.001	-	0.001	0.562	0.001	0.001	-	0.014	0.834	0.026	0.175	-	0.317	0.373	0.434	0.751	-
P4	0.001	0.096	0.001	0.001	0.606	0.001	0.571	0.001	0.001	0.908	0.012	0.754	0.024	0.152	0.914	0.577	0.658	0.651	0.581	0.769
	Campaign 2																			
	A_g					Φ_{PSII}					A_g/R_d					fPAR				
	P1S	P4S	P1	P2	P3	P1S	P4S	P1	P2	P3	P1S	P4S	P1	P2	P3	P1S	P4S	P1	P2	P3
P4S	0.001	-	-	-	-	0.001	-	-	-	-	0.001	-	-	-	-	0.001	-	-	-	-
P1	0.001	0.001	-	-	-	0.001	0.002	-	-	-	0.001	0.608	-	-	-	0.001	0.015	-	-	-
P2	0.001	0.001	0.755	-	-	0.001	0.001	0.603	-	-	0.001	0.938	0.662	-	-	0.001	0.207	0.357	-	-
P3	0.001	0.001	0.193	0.365	-	0.001	0.001	0.125	0.383	-	0.001	0.294	0.598	0.329	-	0.001	0.005	0.001	0.001	-
P4	0.001	0.001	0.337	0.571	0.598	0.001	0.001	0.503	0.986	0.163	0.001	0.191	0.506	0.224	0.961	0.001	0.007	0.001	0.001	0.552

*Table S4: Spectral indices used in this study to estimate carotenoid to total chlorophyll ratio (Car:Chl). The asterisk indicate the two-tailed significance level (ns = P > 0.05, * = P ≤ 0.05, ** = P ≤ 0.01, *** = P ≤ 0.001).*

Spectral Index	Target variable	Model	R^2	Formula	Reference
NPCI	Car:Chl	linear	0.47^{*}	$(R_{680}- R_{430})/(R_{680}+R_{430})$	(Peñuelas *et al.*, 1994)
SIPI	Car:Chl		0.05^{ns}	$(R_{800}-R_{445})/(R_{800}-R_{680})$	(Penuelas *et al.*, 1995)
PSRI	Car:Chl		0^{ns}	$(R_{680}-R_{500})*R_{750}$	(Merzlyak *et al.*, 1999)
$CARI/CI_{red-edge}$	Car:Chl	linear	0.3^{ns}	$((R_{720}-R_{521})/R_{521})/((R_{750}-R_{705})/R_{705})$	(Zhou *et al.*, 2019)
$CRI/CI_{red-edge}$	Car:Chl	linear	0.55^{**}	$((R_{510})^{-1}-(R_{700})^{-1})/((R_{750}-R_{705})/R_{705})$	(Gitelson, 2020)
$CAR_{red-edge}/CI_{red-edge}$	Car:Chl	linear	0.6^{***}	$((R_{510})^{-1}-(R_{700})^{-1}]\times R_{770})/((R_{750}-R_{705})/R_{705})$	This study

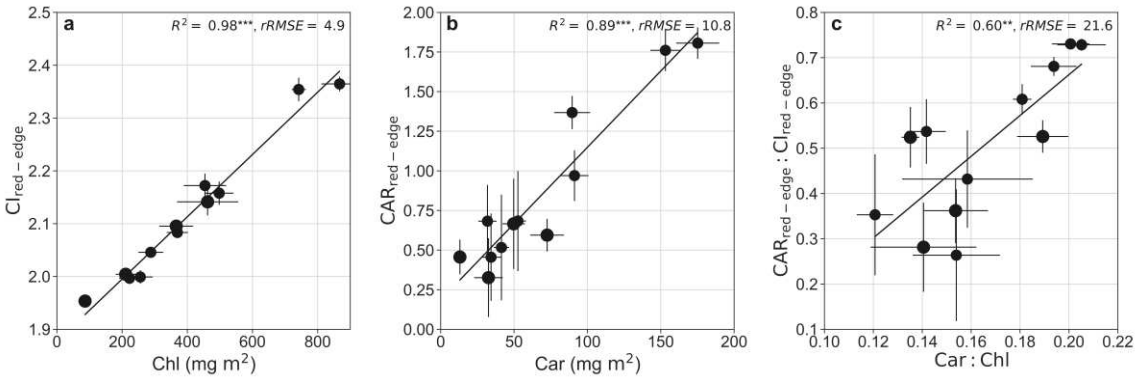

947

948 *Figure S5: (a) Relationship between the red-edge chlorophyll index ($CI_{red-edge}$) and total chlorophyll content*
949 *(Chl). (b) Relationship between the red-edge carotene index ($CAR_{red-edge}$) and carotene content (Car). (c)*
950 *Relationship between the ratio of $CAR_{red-edge}$ to $CI_{red-edge}$ and the ratio of Car to Chl. The black line represents*
951 *the best fitting model for all treatments for both campaigns. Dot colors represent the treatments (green, P4;*
952 *blue, P3; yellow, P2; red, P1), and the crosses represent the treatments without arbuscular mycorrhizal fungi.*
953 *The asterisk indicate the significance level (** = P ≤ 0.01, *** = P ≤ 0.001).*

*Table S5: Pearson coefficient (r) for the correlation of EPS, Car:Chl, sPRI, cPRI and $cPRI_{vi}$. The asterisk indicate the two-tailed significance level (ns = P > 0.05, * = P ≤ 0.05, ** = P ≤ 0.01, *** = P ≤ 0.001).*

	EPS	Car:Chl	sPRI	cPRI	$cPRI_{vi}$
EPS	1	0.743**	-0.753**	**-0.908*** **	-0.873***
Car:Chl	-	1	-0.479ns	-0.742**	-0.622**
sPRI	-	-	1	0.731**	0.902***
cPRI	-	-	-	1	0.900***
$cPRI_{vi}$	-	-	-	-	1

*Table S6: Pearson coefficient (r) for the partial correlation analysis of EPS, Car:Chl, sPRI, cPRI and $cPRI_{vi}$. The table shows the correlation between EPS and sPRI, cPRI and $cPRI_{vi}$ when controlling for their covariance with Car:Chl. The asterisk indicate the two-tailed significance level (ns = P > 0.05, * = P ≤ 0.05, ** = P ≤ 0.01, *** = P ≤ 0.001).*

		Correlation with EPS			
		Car:Chl	sPRI	cPRI	$cPRI_{vi}$
Control variables	Car:Chl	-	-0.676**	**-0.795*** **	-0.784***
	sPRI	0.662**	-	-	-
	cPRI	0.247ns	-	-	-
	$cPRI_{vi}$	0.523*	-	-	-

Semi mechanistic model for estimating Φ_{PSII} by F_{yield} and cPRI

The relationship between Φ_{PSII} and F_{yield} is best described by a 4th order polynomial regression model (see Results). Whereas this model allows the estimation of F_{yield} from Φ_{PSII}, the ambiguity of the polynomial does not allow estimating Φ_{PSII} from F_{yield}, because a single F_{yield} value may correspond with multiple Φ_{PSII} values. To test if this problem can be overcome by combining F_{yield} and cPRI we followed a stepwise process: 1) By calculating the first derivative of this polynomial, the local minimum and maximum can be detected. The local maximum describes the point where the transition from PQ to NPQ as the dominating quenching mechanism of F_{yield} takes place. The local minimum describes the point where photo-damage leads to an increase of F_{yield} under low Φ_{PSII} and high NPQ; 2) by using these transition points, the polynomial is decomposed into three linear models representing the three stress stages; 3) the cPRI as a proxy for EPS was then used to classify F_{yield} into the three stress stages, in the last step 4) the Φ_{PSII} can be estimated from F_{yield} and the linear models found in step two. In the following we refer to this model as the quenching transition point (QTP) model.

The sensitivity and robustness of the QTP model towards the polynomial fit, F_{yield} observation uncertainty and the detection of the stress stages by cPRI was tested by generating 1000 data sets of 12 random samples using Monte Carlo (MC) simulation and the probability-density distribution of the observations. The range of the coefficient of determination (R^2) and relative mean square error (*rRMSE*) of the 1000 datasets were compared to test the reliability of the proposed QTP and cF_{ratio} model (Figure S6). Our results show that even though a combination of F_{yield} and cPRI can be utilized to predict Φ_{PSII}, the model is strongly sensitive to cPRI, where a wrong classification of the stress stages (c.f. Figure 6a&b) results in a strong model bias. For a robust estimation of Φ_{PSII} by F_{yield} a more precise indication of the transition points is thus a necessity.

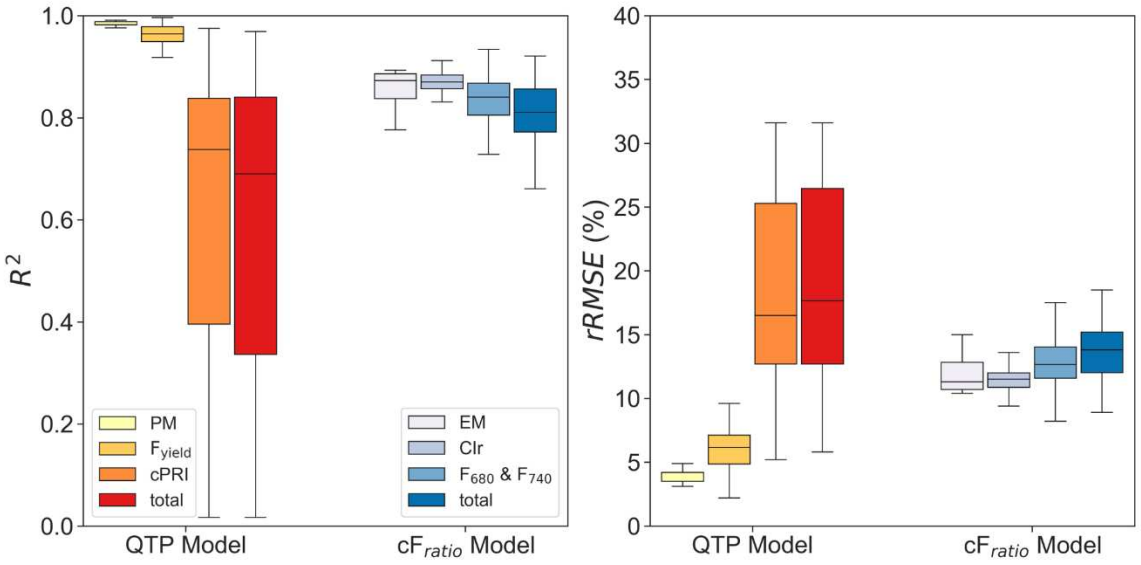

986

987 *Figure S6: Sensitivity of the QTP model towards the polynomial model (PM), fluorescence yield (F_{yield}),*
988 *pigment corrected photochemical reflectance index (cPRI) and a combination of all parameters (total) (red*
989 *box plots). Sensitivity of the cF_{ratio} model towards the exponential model (EM), red-edge chlorophyll index*
990 *(CIr), red and far red fluorescence (F_{685} & F_{740}) and a combination of all parameters (total) (blue box plots).*

991

992

993